ammonium sulfate, 67 mM Tris-HCl (pH 8.8), 6.7 mM $MgCl_2$, 10 mM 2-mercaptoethanol, and 0.001% (w/v) gelatin] and 1.25 units of Ampli-Taq polymerase (Perkin-Elmer Cetus, Norwalk, CT, USA). The PCR products were separated in a 2.0% agarose gel and visualized by staining with ethidium bromide.

Reverse transcription (RT)-PCR

Total RNA was extracted from cells using RNAzolB (TEL-TEST, Friendswood, TX, USA). Three micrograms of total RNA were reverse transcribed by Superscript II (Gibco-BRL, Gaithersburg, MD, USA) using oligo(dT) primer and subjected to PCR. Primers for RT-PCR of SOCS-1 gene expression were as follows: forward, 5′-CACGCACTTCCGCACATTCC-3′; reverse, 5′-TCCAGCAGCTCGAAGAGGCA-3′. For the RT-PCR, the quantity of cDNA template and the number of amplification cycles were optimized to ensure that the reaction was terminated during the linear phase of product amplification, so that semiquantitative comparisons of the mRNA abundance between different samples were possible. RT-PCR with glyceraldehyde phosphate dihydrogenase (GAPDH) primers was done to adjust the amounts of RNA in each experiment.

Statistical analysis

Fisher's exact test was used for statistical evaluation, and P values below 0.05 were considered significant.

Results

Methylation status of SOCS-1 in cultured cell lines

First, the methylation status of the CpG island in the coding region of *SOCS-1* was analyzed in cell lines by MSPCR using the primer sets, HM1F+HM1R and UM1F+UM1R, according to the method of Yoshikawa et al.[15] MSPCR using these primers, however, could not determine the methylation status of the gene: the use of the primers resulted in dimer formation without methylation- or unmethylation-specific bands. We therefore redesigned new sets of primers located in the CpG island of *SOCS-1* (Table 2; HM2F+HM1R for detecting a methylation-specific band and UM2F+UM2R for an unmethylation-specific band). MSPCR with these sets of primers enabled successful detection of methylation- and unmethylation-specific bands in PLC/PRF/5 cells (Fig. 1). The unmethylation-specific band alone was detected in HuH-7 cells, in agreement with the previous report.[15]

Analysis using the primers located in the 5′-noncoding region (see Table 2) yielded a similar pattern, excluding that there were both methylation- and unmethylation-specific bands also in HuH-7 cells (Fig. 1). Accordingly, the primer sets HM2F+HM1R and UM2F+UM2R were used for the analysis of the methylation status of the CpG island, and UMPF-M+UMPR-M and UMPF-U+UMPR-U were used for the 5′-noncoding region, thereafter.

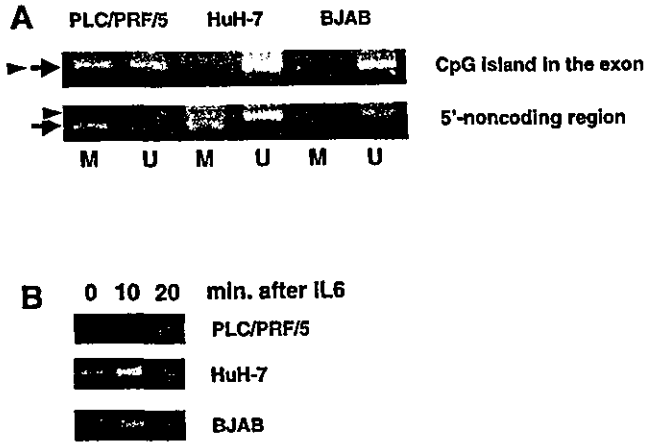

Fig. 1. Genomic and methylation-specific (MSPCR) analysis of cultured hepatoma cell lines in the CpG island and 5′-no-coding region of the *SOCS-1* gene. DNA from human hepatoma cell lines, PLC/PRF/5 and HuH-7, and a B-cell line, BJAB, was analyzed by MSPCR after bisulfite treatment as described in the Patients and methods section. **A** MSPCR with the primers in the CpG island and those in the 5′-noncoding region. **B** RT-PCR showing the expression of SOCS-1 in cell lines before and after the addition of IL-6 (10 ng/ml). The *arrow* indicates the position of the methylation-specific band; the *arrowhead* indicates the position of the unmethylation-specific band. *M*, MSPCR with methylation-specific primers; *U*, MSPCR with unmethylation-specific primers

Expression of SOCS-1 mRNA in cell lines

The expression of SOCS-1 was determined by semiquantitative RT-PCR. Although SOCS-1 expression was abundant in HuH-7 and BJAB cells in the baseline and was enhanced by the addition of IL-6 (10 ng/ml), only marginal expression and no enhancement were detected in PLC/PRF/5 cells. These results are consistent with the methylation status that was determined in the current study and with the expression status in the baseline that was observed in a previous report.[15]

Methylation status of SOCS-1 in human tumor samples

Then, DNA extracted from human HCC and non-HCC tissues was tested for the methylation status of the *SOCS-1* by MSPCR. Only 10 and 6 tissue samples were informative for determining a methylation-specific band

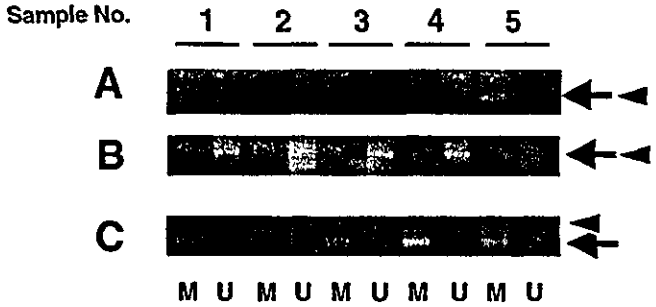

Fig. 2. MSPCR analysis of the CpG island and 5′-noncoding region of the *SOCS-1* from 22 HCC tissue samples. With the same primers used in Fig. 1, 22 pairs of HCC and non-HCC samples were analyzed by MSPCR. Representative cases are shown. Samples *1* and *2* were well-differentiated HCC, *3* and *4* were moderately differentiated HCC, and *5* was poorly differentiated HCC. Panel **B** shows their non-HCC counterparts. **A** MSPCR of DNA from HCC tissue samples with the primers in CpG island. **B** MSPCR of DNA from non-HCC tissue samples with the primers in CpG island. **C** MSPCR of DNA from HCC tissue samples with the primers in 5′-noncoding region. The *arrow* indicates the position of the methylation-specific band; the *arrowhead* indicates the position of the unmethylation-specific band HCC, hepatocellular carcinoma; M, MSPCR with methylation-specific primers; U, MSPCR with unmethylation-specific primers

and an unmethylation-specific band, respectively, when the primers in the CpG island were used. In 9 HCC tissue samples the band indicative of aberrant methylation in the CpG island was detected, while the band indicating unmethylation was detected in 1 HCC tissue sample (Fig. 2). In contrast, in the corresponding non-HCC tissue samples, only 1 exhibited the methylation pattern, whereas the unmethylation pattern was observed in 5 non-HCC tissue samples. Thus, aberrant methylation of *SOCS-1* was significantly associated with HCC rather than with non-HCC tissues ($P = 0.0076$ by Fisher's exact test).

Using primers in the 5′-noncoding promoter region, 14 and 15 HCC tissue samples were informative for a methylation-specific band and an unmethylation-specific band, respectively. Aberrant methylation was observed in 12 HCC tissue samples whereas the unmethylation pattern was detected in 5 HCC tissue samples. In contrast, only 2 non-HCC tissues exhibited aberrant methylation whereas the unmethylation pattern was detected in 10 non-HCC tissues: there was also a significant correlation between HCC and aberrant methylation of *SOCS-1* ($P = 0.0042$).

Neither a methylation-specific nor an unmethylation-specific band in 12 HCC and 16 non-HCC tissues was detected using the primers in the CpG island and in 5 HCC and 10 non-HCC tissue samples using the primers in the 5′-noncoding promoter region, suggesting that *SOCS-1* in these tissues was in a mosaic state of methylation. This suggestion was examined using a hepatoma cell line HLF: neither a methylation- nor an unmethylation-specific band was detected, but after 5-azacytidine treatment of the cell line for 3 days, which cancels methylation of the gene,[22] an unmethylation-specific band appeared, demonstrating that *SOCS-1* in the cell line is methylated in a mosaic fashion. Consequently, *SOCS-1* gene expression was turned on as determined by RT-PCR.

Correlation between SOCS-1 methylation and clinicopathological findings

The relationship between the methylation status of *SOCS-1* and clinicopathological findings is shown in Table 1. When the methylation status in HCC tissue samples was correlated with parameters such as the presence or absence of cirrhosis as the underlying liver disease, the histological degree of HCC, tumor sizes, vascular invasion, distant metastasis, or tumor stages, no significant association was noted.

Discussion

In the current study, we analyzed the methylation status of *SOCS-1*, a negative regulator of the JAK/STAT pathway, by the MSPCR method. Using the primers located in the CpG island in the coding region, aberrant methylation was observed in 9 of 22 (41%) HCC tissue samples, and 12 of 22 (54.5%) HCC tissue samples by the use of primers in the 5′-noncoding region. The former rate is almost compatible with the incidence in a previous report.[14] It is notable that a similar or higher rate of aberrant methylation was detected in the 5′-noncoding promoter region of *SOCS-1*. It is established that methylation in the promoter region is essential in the regulation of (silencing) the genes.[16,17] The frequent occurrence of aberrant methylation in the promoter region of *SOCS-1* further supports the notion that the downregulation of SOCS-1 expression is common in human HCC. Very recently, methylation in the promoter of SOCS-1 gene was reported in pancreatic tumors.[23]

In our MSPCR analysis, a substantial number of samples showed neither the methylated nor unmethylated pattern. The reason for this dual negativity is unclear. One possibility is a mosaic methylation pattern that may exist in the *SOCS-1*. If not all the susceptible cytosine residues are methylation, i.e., a gene is methylated in a mosaic fashion, one cannot determine the methylation status by MSPCR. This possibility was confirmed using a hepatoma cell line, as shown in the Results section. Neither a methylation- nor an unmethylation-specific band was detected, but after

5-azacytidine treatment of the cell line for 3 days, which cancels methylation of the gene,[22] an unmethylation-specific band appeared, demonstrating that *SOCS-1* in the cell line is methylated in a mosaic fashion.

SOCS-1 transcription is activated by signal transducer and activator of transcription (STAT) and the resultant proteins negatively regulate the JAK/STAT pathways either by directly inhibiting JAKs or by binding to receptors and blocking further association with STATs. Of the eight SOCS family members, SOCS-1 is a negative regulator of IL-6 signals. The silencing of *SOCS-1* results in constitutive activation of the JAK/STAT pathway. Without negative feedback by SOCS-1, the downstream pathways and target genes are strongly activated.[24] There are several lines of evidence supporting the idea that the JAK/STAT pathway may be involved in oncogenesis. The constitutive activation of the JAK/STAT pathway including STAT3 is observed in a number of transformed cells.[25] Thus, SOCS-1 is considered to be a tumor suppressor candidate, which chiefly has a role in the development of hematopoietic malignancies.[26] Also, an association of the SOCS-1 in hepatocarcinogenesis has recently been suggested.[15] There are a variety of gene products in the downstream of the JAK/STAT pathway, including c-*myc* or c-*fos*.[27] The activation of the pathway thus may cause an activation of oncogenes or growth-associated genes and eventually lead to oncogenesis. The precise role of SOCS-1 in hepatocarcinogenesis is currently unclarified and requires further study, but it might play an essential role in the majority of HCCs.

Our current results confirmed those of a previous study[14] and added a new piece of information on methylation of the promoter region of *SOCS-1*. However, the presence of cases negative for both methylation and unmethylation may limit the application of this technique for the analysis of hepatocarcinogenesis. In addition, recently the association between the core protein of hepatitis C virus and the JAK/STAT pathway has been reported as a potential proliferator of hepatocytes.[28] Besides aberrant methylation, association of SOCS-1 with HCV may cause a down-regulation of *SOCS-1* expression. In relation to this issue, it is interesting to note that a few patients in our series exhibited aberrant methylation of *SOCS-1* in the adjacent non-HCC tissue samples. Infection with HCV, which is present in all patients, may be associated with *SOCS-1* expression in human HCC tissues. Further studies are necessary for deciphering the complicated involvement of the SOCS-1 and JAK/STAT pathway in hepatocarcinogenesis, possibly in association with HCV infection.

References

1. Chen CJ, Yu MW, Liaw YF. Epidemiological characteristics and risk factors of hepatocellular carcinoma. J Gastroenterol Hepatol 1997;12:S294–308.
2. Saito I, Miyamura T, Ohbayashi A, Harada H, Katayama T, Kikuchi S, et al. Hepatitis C virus infection is associated with the development of hepatocellular carcinoma. Proc Natl Acad Sci U S A 1990;87:6547–9.
3. Robinson WS. Molecular events in the pathogenesis of hepadnavirus-associated hepatocellular carcinoma. Annu Rev Med 1994;45:297–323.
4. Umeda T, Hino O. Molecular aspects of human hepatocarcinogenesis mediated by inflammation: from hypercarcinogenic state to normo- or hypocarcinogenic state. Oncology 2002;62:38–42.
5. Kim CM, Koike K, Saito I, Miyamura T, Jay G. HBx gene of hepatitis B virus induces liver cancer in transgenic mice. Nature (Lond) 1991;351:317–20.
6. Moriya K, Fujie H, Shintani Y, Yotsuyanagi H, Tsutsumi T, Matsuura Y, et al. The core protein of hepatitis C virus induces hepatocellular carcinoma in transgenic mice. Nat Med 1998; 41065–7.
7. Lerat H, Honda M, Beard MR, Loesch K, Sun J, Yang Y, et al. Steatosis and liver cancer in transgenic mice expressing the structural and nonstructural proteins of hepatitis C virus. Gastroenterology 2002;122:352–65.
8. Koike K, Tsutsumi T, Fujie H, Shintani Y, Moriya K. Role of hepatitis viruses in hepatocarcinogenesis. Oncology 2002;62:29–37.
9. Satoh S, Daigo Y, Furukawa Y, Kato T, Miwa N, Nishiwaki T, et al. AXIN1 mutations in hepatocellular carcinomas, and growth suppression in cancer cells by virus-mediated transfer of AXIN1. Nat Genet 2000;24:245–50.
10. Fujie H, Moriya K, Shintani Y, Tsutsumi T, Takayama T, Makuuchi M, et al. Frequent β-catenin aberration in human hepatocellular carcinoma. Hepatol Res 2001;20:39–51.
11. Matsuda Y, Ichida T, Matsuzawa J, Sugimura K, Asakura H. p16(INK4) is inactivated by extensive CpG methylation in human hepatocellular carcinoma. Gastroenterology 1999;116:394–400.
12. Starr R, Willson TA, Viney EM, Murray LJ, Rayner JR, Jenkins BJ, et al. A family of cytokine-inducible inhibitors of signaling. Nature (Lond) 1997;387:917–21.
13. Endo TA, Masuhara M, Yokouchi M, Suzuki R, Sakamoto H, Mitsui K, et al. A new protein containing an SH2 domain that inhibits JAK kinases. Nature 1997;387:921–4.
14. Naka T, Matsumoto T, Narazaki M, Fujimoto M, Morita Y, Ohsawa Y, et al. Accelerated apoptosis of lymphocytes by augmented induction of Bax in SSI-1 (STAT-induced STAT inhibitor-1) deficient mice. Proc Natl Acad Sci U S A 1998;95: 15577–82.
15. Yoshikawa H, Matsubara K, Qian GS, Jackson P, Groopman JD, Manning JE, et al. SOCS-1, a negative regulator of the JAK/STAT pathway, is silenced by methylation in human hepatocellular carcinoma and shows growth-suppression activity. Nat Genet 2001;28:29–35.
16. Jaenisch R, Bird A. Epigenetic regulation of gene expression: how the genome integrates intrinsic and environmental signals. Nat Genet 2003;33:245–54.
17. Herman JG, Baylin SB. Promoter-region hypermethylation and gene silencing in human cancer. Curr Top Microbiol Immunol 2000;249:35–54.
18. Desmet VJ, Gerber M, Hoofnagle JH, Manns M, Scheuer PJ. Classification of chronic hepatitis: diagnosis, grading and staging. Hepatology 1994;19:1513–20.
19. Hermanek P, Sobin LH. UICC TNM classification of malignant tumors. 4th ed. Berlin: Splinger; 1987.
20. Yotsuyanagi H, Yasuda K, Iino S, Moriya K, Fujie H, Shintani Y, et al. Persistent viremia after recovery from self-limited acute hepatitis B. Hepatology 1998;27:1377–82.

21. Herman JG, Graff JR, Myohanen S, Nelkin BD, Baylin SB. Methylation-specific PCR: a novel PCR assay for methylation status of CpG islands. Proc Natl Acad Sci U S A 1996;93:9821–6.
22. Velicescu M, Weisenberger DJ, Gonzales FA, Tsai YC, Nguyen CT, Jones PA. Cell division is required for de novo methylation of CpG islands in bladder cancer cells. Cancer Res 2002;62:2378–84.
23. House MG, Guo M, Iacobuzio-Donahue C, Herman JG. Molecular progression of promoter methylation in intraductal papillary mucinous neoplasms (IPMN) of the pancreas. Carcinogenesis (Oxf) 2003;24:193–8.
24. Greenhalgh CJ, Miller ME, Hilton DJ, Lund PK. Suppressors of cytokine signaling: relevance to gastrointestinal function and disease. Gastroenterology 2002;123:2064–81.
25. Kishimoto T, Kikutani H. Knocking the SOCS off a tumor suppressor. Nat Genet 2001;28:4–5.
26. Rottapel R, Ilangumaran S, Neale C, La Rose J, Ho JM, Nguyen MH, et al. The tumor suppressor activity of SOCS-1. Oncogene 2002;21:4351–62.
27. Darnell JE Jr, Kerr IM, Stark GR. Jak-STAT pathways and transcriptional activation in response to IFNs and other extracellular signaling proteins. Science 1994;264:1415–21.
28. Yoshida T, Hanada T, Tokuhisa T, Kosai K, Sata M, Kohara M, et al. Activation of STAT3 by the hepatitis C virus core protein leads to cellular transformation. J Exp Med 2002;196:641–53.

GASTROENTEROLOGY 2004;126:840–848

BASIC–LIVER, PANCREAS, AND BILIARY TRACT

Hepatitis C Virus Infection and Diabetes: Direct Involvement of the Virus in the Development of Insulin Resistance

YOSHIZUMI SHINTANI,* HAJIME FUJIE,* HIDEYUKI MIYOSHI,* TAKEYA TSUTSUMI,* KAZUHISA TSUKAMOTO,† SATOSHI KIMURA,* KYOJI MORIYA,* and KAZUHIKO KOIKE*
Departments of *Internal Medicine and †Metabolic Diseases, Graduate School of Medicine, University of Tokyo, Tokyo, Japan

See editorial on page 917.

Background & Aims: Epidemiological studies have suggested a linkage between type 2 diabetes and chronic hepatitis C virus (HCV) infection. However, the presence of additional factors such as obesity, aging, or cirrhosis prevents the establishment of a definite relationship between these 2 conditions. *Methods:* A mouse model transgenic for the HCV core gene was used. *Results:* In the glucose tolerance test, plasma glucose levels were higher at all time points including in the fasting state in the core gene transgenic mice than in control mice, although the difference was not statistically significant. In contrast, the transgenic mice exhibited a marked insulin resistance as revealed by the insulin tolerance test, as well as significantly higher basal serum insulin levels. Feeding with a high-fat diet led to the development of overt diabetes in the transgenic mice but not in control mice. A high level of tumor necrosis factor-α, which has been also observed in human chronic hepatitis C patients, was considered to be one of the bases of insulin resistance in the transgenic mice, which acts by disturbing tyrosine phosphorylation of insulin receptor substrate-1. Moreover, administration of an anti-tumor necrosis factor-α antibody restored insulin sensitivity. *Conclusions:* The ability of insulin to lower the plasma glucose level in the HCV transgenic mice was impaired, as observed in chronic hepatitis C patients. These results provide a direct experimental evidence for the contribution of HCV in the development of insulin resistance in human HCV infection, which finally leads to the development of type 2 diabetes.

Approximately 200 million people are chronically infected with hepatitis C virus (HCV) in the world. Chronic HCV infection may lead to cirrhosis and hepatocellular carcinoma, thereby being a worldwide problem both in medical and socioeconomical aspects.[1,2] In addition, chronic HCV infection is a multifaceted disease, which is associated with numerous clinical manifestations, such as essential mixed cryoglobulinemia, porphyria cutanea tarda, and membranoproliferative glomerulonephritis.[3] Recent epidemiological studies have added another clinical condition, type 2 diabetes, to a spectrum of HCV-associated diseases.[4–7] However, the establishment of a definite causative relationship between HCV infection and diabetes is hampered by the presence of other factors such as obesity, aging, or liver injury in patients with chronic HCV infection.

Type 2 diabetes is a complex, multisystem disease with a pathophysiology that includes a defect in insulin secretion, increased hepatic glucose production, and resistance to the action of insulin, all of which contribute to the development of overt hyperglycemia.[8,9] Although the precise mechanisms whereby these factors interact to produce glucose intolerance and diabetes are uncertain, it has been suggested that the final common pathway responsible for the development of type 2 diabetes is the failure of the pancreatic β-cells to compensate for the insulin resistance. Hyperinsulinemia in the fasting state is observed relatively early in type 2 diabetes, but it is considered to be a secondary response that compensates for the insulin resistance.[8,9] Overt diabetes occurs over time when pancreatic β-cells bearing the burden of increased insulin secretion fail to compensate for the insulin resistance.

In this study, to elucidate the role of HCV in a possible association between diabetes and HCV infection, transgenic mice that carry the core gene of HCV[10,11] were analyzed. We found that these mice developed insulin resistance. An addition of a high-calorie diet led to the development of type 2 diabetes by dis-

Abbreviations used in this paper: EDL, extensor digitorum longus; ELISA, enzyme-linked immunosorbent assay; FPG, fasting plasma glucose; HCV, hepatitis C virus; IRS, insulin receptor substrate; JNK, c-Jun N-terminal kinase; TNF-α, tumor necrosis factor-α.

© 2004 by the American Gastroenterological Association
0016-5085/04/$30.00
doi:10.1053/j.gastro.2003.11.056

rupting the balance between insulin resistance and secretion.

Materials and Methods

Transgenic Mice

The production of HCV core gene transgenic mice has been described previously.[11] Briefly, the core gene from HCV of genotype 1b, which is placed downstream of a transcriptional regulatory region from the hepatitis B virus, was introduced into C57BL/6 mouse embryos (Clea Japan, Tokyo, Japan). The mice were cared for according to institutional guidelines, fed an ordinary chow diet (Funabashi Farms, Funabashi, Japan), and maintained in a specific pathogen-free state. At an indicated time, the mice were fed a high-fat diet (Oriental Yeast Co., Ltd., Tokyo, Japan) for up to 2 months. Caloric content of food was 4.70 kcal/g for high-fat diet and 3.56 kcal/g for ordinary diet. The high-fat diet contains 18.5% protein, 22.1% fat (4.7% vegetable fat and 17.4% animal fat), 5.4% ash, 2.5% fiber, 6.5% moisture, and 45.0% carbohydrate, and the ordinary diet contains 22.4% protein, 5.7% fat, 6.6% ash, 3.1% fiber, 7.7% moisture, and 54.5% carbohydrate. Because there is a sex preference in the development of liver lesion in the transgenic mice, we used only male mice that were heterozygously transgenic for the core gene, and as controls we used nontransgenic litter mates of the transgenic mice. Transgenic mice carrying the HCV envelope genes under the same regulatory region as that in the core gene transgenic mice were also used as controls.[12] At least 5 mice were used in each experiment and the data were subjected to statistical analysis.

Glucose Tolerance Test

The mice were fasted for >16 hours before the study. D-Glucose (1g/kg body weight) was administered by intraperitoneally (IP) injection to conscious mice. Blood was drawn at different time points from the orbital sinus, and plasma glucose concentrations were measured by using an automatic biochemical analyzer DRI-CHEM 3000V (Fuji Film, Tokyo, Japan). The levels of serum insulin were determined by radioimmunoassay (BIOTRAK; Amersham Pharmacia Biotech, Piscataway, NJ) with rat insulin as a standard.

Insulin Tolerance Test

The mice were fed freely and then fasted during the study period. Human insulin (1 U/kg body weight) (Humulin; Novo Nordisk, Denmark) was administered by IP injection to fasted conscious mice, and glucose concentrations were determined at the time points indicated. Values were normalized to the baseline glucose concentration at the administration of insulin.

Morphometric Analysis

Sections of the pancreas were prepared and evaluated for morphometry after H&E staining or immunostaining. Relative islet area and islet number were determined with an image analyzer (QUE-2; Olympus Optical Co., Tokyo, Japan).

Enzyme-Linked Immunosorbent Assay

ELISA for mouse tumor necrosis factor (TNF)-α was performed using a commercially available mouse TNF-α ELISA kit (BioSource International, Camarillo, CA). Samples were prepared as reported previously.[13] Briefly, the liver of transgenic and control mice were lysed with a buffer containing 1% Tween 80, 10 mmol/L Tris-HCl [pH 7.4], 1 mmol/L EDTA, 0.05% sodium azide, 2 mmol/L PMSF, and the Protease Inhibitor Cocktail (Complete; Roche Molecular Biochemicals, Indianapolis, IN) and homogenized on ice for 20 seconds. The homogenates were centrifuged at 11,000 × *g* for 10 minutes at 4° C, and the supernatants were collected and assayed. ELISA was performed in triplicate for each sample. The concentrations of the cytokines in the liver were normalized by determining the amount of total protein in each sample using the BCA Protein Assay Kit (Pierce, Rockford, IL).

Immunoprecipitation and Western Blotting

For immunoprecipitation studies, liver tissues were homogenized in lysis buffer (10 mmol/L Tris-HCl at pH 7.5, 150 mmol/L NaCl, 10 mmol/L sodium pyrophosphate, 1.0 mmol/L β-glycerophosphate, 1.0 mmol/L sodium orthovanadate [Na_3VO_4], 50 mmol/L sodium fluoride [NaF], the Protease Inhibitor Cocktail [Complete, Roche Molecular Biochemicals], and 1.0% Triton X-100), and homogenates were precipitated with an anti–insulin receptor substrate (IRS)-1 or anti–IRS-2 rabbit polyclonal antibody (UBI, Lake Placid, NY) and then with Sepharose 4B beads (Amersham Biosciences). Resulting pellets were washed 3 times and then subjected to Western blotting. Pellets were resuspended in Western sample buffer (5% β-mercaptoethanol, 2% sodium dodecyl sulfate, 62.5 mmol/L Tris-HCl, 1 mmol/L EDTA, 10% glycerol), and then subjected to 2%–15% gradient sodium dodecyl sulfate/PAGE (PAG Mini "DAIICHI" 2/15 (13W), Daiichi Diagnostics, Tokyo, Japan), and electrotransferred to polyvinylidene difluoride membranes (Immobilon-P, Millipore, Bedford, MA). The filter was then reacted with antiphosphorylated tyrosine (Santa Cruz Biotechnology Inc., Santa Cruz, CA), antiphosphorylated serine (Cell Signaling Technology, Inc., Beverly, MA), anti–IRS-1 or anti–IRS-2 mouse monoclonal antibody (BD Biosciences, Lexington, KY), followed by immunostaining with secondary biotinylated IgG (Vector Labs, Inc., Burlingame, CA) and visualization using an ECL kit (Amersham Intl., Buckinghamshire, UK).[14]

Hyperinsulinemic-Euglycemic Clamp

Mice underwent a hyperinsulinemic-euglycemic clamp using D-[3-^{3}H]glucose (NEN Life Science, Boston, MA) to measure the rate of glucose appearance and hepatic glucose production (HGP) as described previously.[15] Three days after jugular catheter placement, a hyperinsulinemic-euglycemic clamp was conducted with a continuous infusion of human

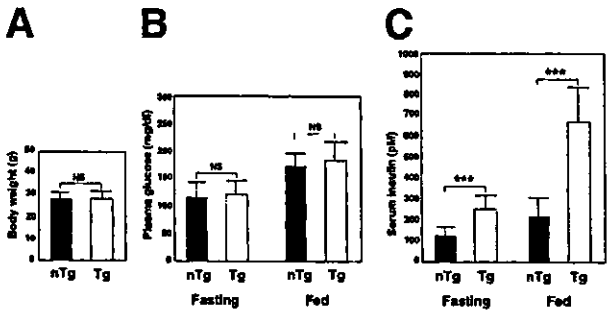

Figure 1. Altered glucose homeostasis in hepatitis C virus core gene transgenic mice. (*A*) Body weight of 2-month-old mice (n = 10 in each group). (*B*) Plasma glucose levels in fasting or fed mice (n = 10 in each group). (*C*) Serum insulin levels in fasting or fed mice (n = 10 in each group). The insulin level was significantly higher in the core gene transgenic mice than in control mice. Values are mean ± standard error; $***P < 0.001$; NS, statistically not significant; nTg, nontransgenic mice; Tg, transgenic mice.

insulin to raise serum insulin within a physiological range. Blood samples were drawn at intervals for the immediate measurement of blood glucose concentration, and 20% glucose was infused at variable rates to maintain blood glucose at ca. 125 mg/dL. All infusions were done using microdialysis pumps (KD Scientific Inc., Boston, MA). The rate of glucose appearance (mg/kg per minute), which equals the rate of total body glucose utilization during steady state, was calculated as the ratio of the rate of infusion of [3-^{3}H]glucose and the steady state plasma [^{3}H-]glucose specific activity. HGP (mg/kg/min) during clamps was determined by subtracting the glucose infusion rate from the rate of glucose appearance.

Glucose Uptake by Skeletal Muscle

The extensor digitorum longus (EDL) or soleus muscle was excised from 2-month-old mice and exposed to insulin at the indicated concentrations. 2-Deoxyglucose uptake was determined as described previously.[16]

Treatment With Anti-TNF-α Antibody

To suppress TNF-α, a dose of 200 μg/mouse of neutralizing hamster monoclonal antibody (TN3-19.12, Santa Cruz Biotechnology Inc.) was administered by IP injection on days 1 and 4, and plasma glucose and insulin levels were determined at day 5.[17]

Statistical Analysis

The results are expressed as means ± standard error. The significance of the difference in means was determined by Student *t* test or Mann–Whitney *U* test whenever appropriate. $P < 0.05$ was considered significant.

Results

Hyperinsulinemia and Insulin Resistance in Transgenic Mice

At the age between 1 and 12 months, there was no significant difference in body weight between the core gene transgenic mice and control mice. Figure 1*A* shows body weight of 2-month-old mice. Fasting plasma glucose (FPG) levels were slightly elevated in the core gene transgenic mice compared with control mice, but the difference was not significant ($P = 0.79$, Figure 1*B*). In contrast, there was a marked increase in the level of serum insulin in the core gene transgenic mice than control mice ($P < 0.001$, Figure 1*C*). Hyperinsulinemia was observed in the core gene transgenic mice as early as 1 month old. These findings suggest that decreased responsiveness to the hormone may have resulted in compensatory hyperinsulinemia. Administration of glucose to 2-month-old core gene transgenic mice revealed mild glucose intolerance compared with control mice of the same age, but the difference was not statistically significant at any time points measured (Figure 2*A*). HCV envelope gene transgenic mice of the same age, in which the envelope genes were expressed under the same transcriptional regulatory region as the core gene transgenic mice, did not manifest hyperinsulinemia or elevated FPG levels, indicating that not the transcriptional regulatory region used but the expressed gene itself is essential in this phenotype.

The insulin tolerance test conducted at the age of 2 months revealed that the reduction in plasma glucose concentration after IP insulin injection was impaired in the core gene transgenic mice, displaying higher plasma glucose levels than those in control mice at all time points measured (Figure 2*B*). At 40 and 60 minutes, the difference was statistically significant between transgenic

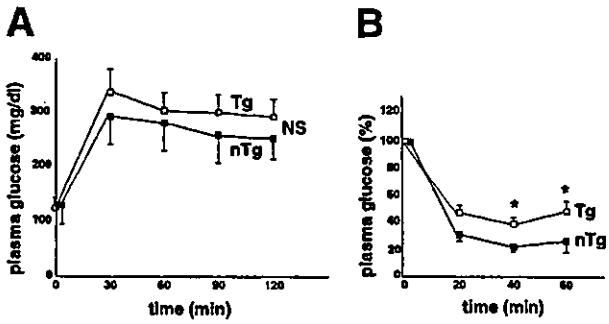

Figure 2. Insulin resistance in the core gene transgenic mice. (*A*) Glucose tolerance test (n = 5 in each group). Animals were fasted overnight (>16 hours). D-Glucose (1 g/kg body weight) was administered by IP injection to conscious mice, and plasma glucose levels were determined at the time points indicated. (*B*) Insulin tolerance test (n = 5 in each group). Human insulin (1 U/kg body weight) was administered by IP injection to fasted conscious mice and glucose concentrations were determined. Values were normalized to the baseline glucose concentration at the time of insulin administration. Values are mean ± standard error; $*P < 0.05$; NS, statistically not significant; nTg, nontransgenic mice; Tg, transgenic mice.

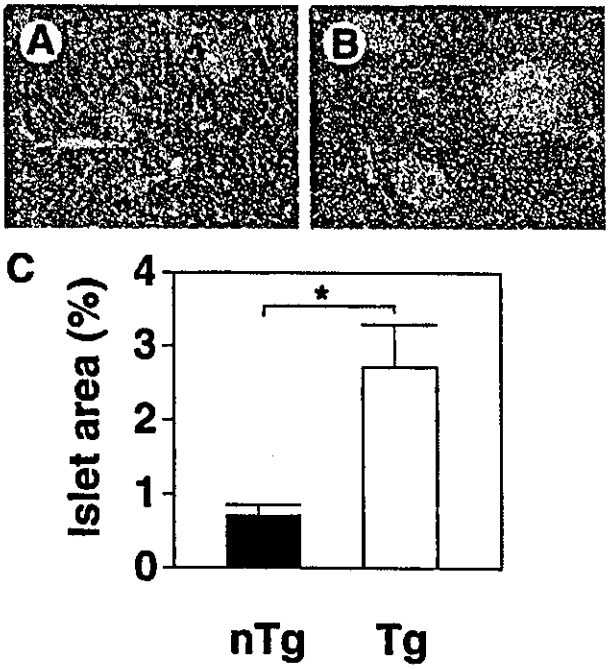

Figure 3. Analysis of pancreatic islet mass in the core gene transgenic and control mice. (*A* and *B*) Morphology of representative islets (H&E staining) from normal control mice (*A*) or the core gene transgenic mice (*B*). (*C*) Relative islet area, expressed as a percentage of the total stained pancreatic section, for control mice (nTg) and the core gene transgenic mice (Tg) (n = 10 in each group). Values are mean ± standard error; $*P < 0.05$.

and control mice (39.6 ± 1.3 vs. 24.4 ± 1.1 and 43.7 ± 2.1 vs. 26.4 ± 2.3, $P < 0.05$). These data are consistent with a defect in the actions of insulin on glucose disposal and/or production in the core gene transgenic mice.

Morphology of Pancreatic Islet Cells

Because a critical factor contributing to whether insulin resistance progresses to diabetes is the capacity of the pancreatic β-cells to respond to increased demands for insulin secretion, we evaluated the morphology of pancreatic islet cells by histologic examination. In the pancreas of HCV core gene transgenic mice, an approximately 3-fold increase in islet mass was observed (Figure 3, $P < 0.05$), which is consistent with β-cell compensation to insulin resistance. There was no infiltration of inflammatory cells within or surrounding the islets.

Feeding Transgenic Mice a High-Fat Diet Leads to Overt Diabetes

Thus, an insulin resistance is present but no apparent glucose intolerance (overt diabetes) in the HCV core gene transgenic mice. This is probably because of the genetic background of C57BL/6 mice, which has been shown to maintain either normal or mildly elevated glucose levels despite insulin resistance.[18] To determine whether a high-fat diet exacerbates the prediabetic phenotype, 2-month-old HCV core gene transgenic mice were fed a high-fat diet for up to 8 weeks. Both the transgenic and control mice showed a similar increase (about 30%) in body weight (Figure 4*A*). After 8 weeks on this diet, 100% (10 out of 10) of the transgenic mice exhibited casual (fed) plasma glucose levels >250 mg/dL, whereas none of the 10 control mice fed the same diet exhibited levels >250 mg/dL (325.0 ± 66.6 vs. 179.0 ± 17.4 mg/dL, $P < 0.01$, Figure 4*B*). Insulin levels were significantly higher in the core gene transgenic mice than in control mice both at fasting and fed state (Figure 4*C*, $P < 0.01$ and $P < 0.001$). In control mice, serum insulin levels in high-fat diet state were significantly higher than those in normal diet state at fed state (Figures 1*C* and 4*C*, $P < 0.01$). Although FPG levels were not significantly different between the transgenic and control mice, these results indicate that feeding a high-fat diet leads to the development of overt diabetes in a mouse model for HCV infection. Body weight gain, particularly with high levels of lipid, may trigger the process leading to overt diabetes in an insulin resistance model mouse with compensatory hyperplasia of islet cells.

Insulin Resistance in the Core Gene Transgenic Mice Is Chiefly Caused by Hepatic Insulin Resistance

We then investigated the mechanism of insulin resistance in the core gene transgenic mice. There was no

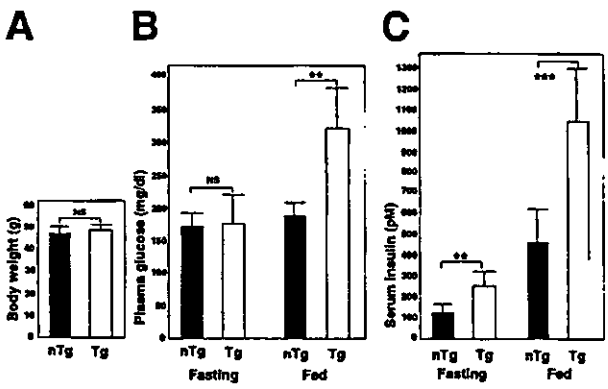

Figure 4. Body weight and glucose homeostasis after a high-fat diet. Control and transgenic mice were fed a high-fat diet for 8 weeks; thereafter, body weight and blood parameters were determined. (*A*) Body weight at the end of the high-fat diet (n = 10 in each group). (*B*) Plasma glucose levels determined in a fasting or fed state (n = 10 in each group). (*C*) Serum insulin levels in a fasting or fed state (n = 10 in each group). Values are mean ± standard error; NS, statistically not significant; $**P < 0.01$; $***P < 0.001$; nTg, nontransgenic mice; Tg, transgenic mice.

significant difference in body weight between the transgenic and control mice as already shown in Figure 1*A*. After the age of 3 months, the core gene transgenic mice developed hepatic steatosis, which is known to be one of the causes of insulin resistance in humans.[19] However, in 1-month-old mouse livers that were used in the analysis of insulin resistance, no hepatic steatosis was noted. No difference was observed in the levels of free fatty acids in the sera between the transgenic and control mice (0.56 ± 0.33 vs. 0.50 ± 0.21 mmol/L, n = 7 in each group, P = 0.65).

Then, we explored the role of the liver in pathogenesis of insulin resistance in the core gene transgenic mice. To directly measure HGP, the hyperinsulinemic-euglycemic clamp technique was conducted as described in Materials and Methods. The core gene transgenic mice showed a normal or slightly lower rate of HGP during the basal period as compared with control mice (Figure 5*A*). Although insulin infusion during the clamp suppressed HGP by 60% in the control mice, insulin induced little effect on HGP of the core gene mice (Figure 5*A*). This is consistent with the notion that insulin resistance in the core gene transgenic mice is chiefly depending on the shortage of insulin action on the liver.

To study the involvement of muscles in the development of insulin resistance in the core gene transgenic mice, we then examined whether or not insulin-stimulated glucose uptake is impaired in the skeletal muscles. The extensor digitorum longus muscle (EDL) from 2-month-old core gene transgenic and control mice were excised and exposed to insulin at the intermediate (0.30 nmol/L) and maximal (10.0 nmol/L) concentrations. There was no significant difference in 2-deoxyglucose uptake in the EDL muscle between the core gene transgenic mice and control mice at either insulin concentration (Figure 5*B*, at 0.30 nmol/L, P = 0.23 and at 10.0 nmol/L, P = 0.76). As another representative muscle that differs from EDL in metabolic properties, the soleus muscle was examined in the same manner as EDL. 2-Deoxyglucose uptake by the soleus muscle was not significantly different between the core gene transgenic and control mice (Figure 5*C*, at 0.30 nmol/L, P = 0.49 and at 10.0 nmol/L, P = 0.49). Thus, in the core gene transgenic mice, contribution of the peripheral skeletal muscle in the development of insulin resistance is negligible. This is in agreement with the observation that the core protein was exclusively present in the liver as detected by Western blotting,[20] which was confirmed by a sensitive enzyme immunoassay (Tsutsumi T. et al., unpublished data, December 2002).[21]

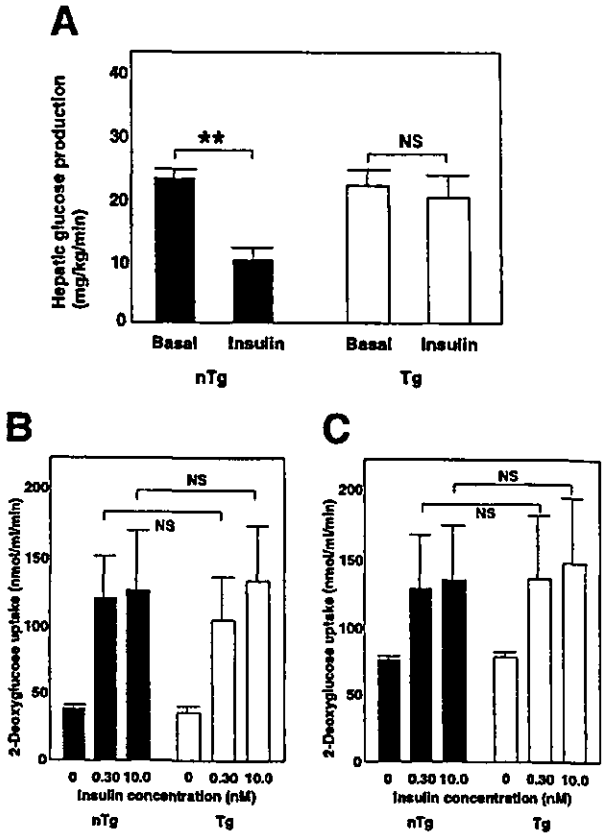

Figure 5. Characterization of glucose metabolism in the core gene transgenic mice. (*A*) Hyperinsulinemic-euglycemic clamp. Hepatic glucose production was calculated using hyperinsulinemic-euglycemic clamp. There was a failure of insulin to suppress hepatic glucose production in the core gene transgenic mice (n = 5 in each group). (*B* and *C*) Glucose uptake by the muscle after insulin stimulation. The extensor digitorum longus muscle (*A*) or soleus muscle (*B*) of 2-month-old mice were excised and exposed to insulin at intermediate (0.30 nmol/L) and maximal (10.0 nmol/L) concentrations. 2-Deoxyglucose uptake was determined as described in the Materials and Methods section (n = 8 in each group). Values are mean ± standard error; NS, statistically not significant; nTg, nontransgenic mice; Tg, transgenic mice.

Elevated TNF-α Level and Altered Tyrosine Phosphorylation of Insulin Receptor Substrate-1 in the Liver and Insulin Resistance

We have noted an increase in TNF-α levels in the liver of HCV core gene transgenic mice,[13] which has also been documented in the sera of human hepatitis C patients.[22–25] On the other hand, TNF-α has been shown to induce insulin resistance in experimental animals and cultured cells.[26–29] Therefore, we next determined the protein expression level of TNF-α by ELISA in the liver of these mice that were used in the current study. The TNF-α levels in the liver of 2-month-old transgenic mice were 702.2 ± 283.3 pg/mg protein and 313.5 ±

113.6 pg/mg protein in that of 2-month-old control mice (n = 10 in each group, $P < 0.001$). Thus, the levels of TNF-α exhibited a more than 2-fold increase in the HCV core gene transgenic mice compared with the control mice, which may be associated with insulin resistance.

Suppression of tyrosine phosphorylation of IRS-1 and -2 is one of the mechanisms by which a high level of TNF-α causes insulin resistance.[29-31] We, therefore, examined the suppression of tyrosine phosphorylation of IRS-1 in response to insulin action in the core gene transgenic mice. Twenty minutes after the administration of human insulin (1 U/kg body weight), when the plasma glucose levels decreased (Figure 2*B*), IRS-1 in the liver of control mice exhibited a marked phosphorylation of its tyrosine. In contrast, phosphorylation level of tyrosine in IRS-1 in the liver of core gene transgenic mice manifested apparently no increase compared with the basal level after the administration of insulin (Figure 6). In contrast, there was no difference in the time course of tyrosine phosphorylation of IRS-2 between the core gene transgenic and control mice (data not shown). These results indicate that a suppression of tyrosine phosphorylation of IRS-1, that is, a suppression of the insulin action in the liver, is at least one of the mechanisms of insulin resistance in HCV transgenic mice, whereas pathways other than IRS-1 may also be involved.

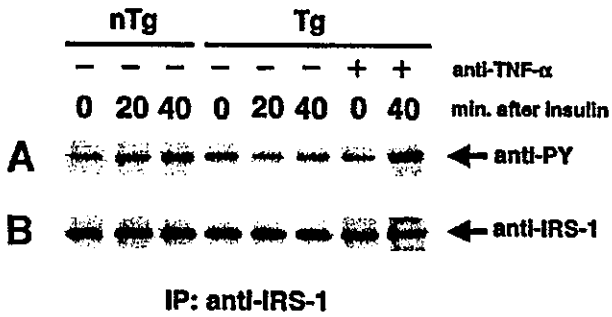

Figure 6. Phosphorylation of tyrosine in IRS-1 in response to insulin stimulation. Liver tissues from control mice and core gene transgenic mice with or without anti-TNF-α antibody treatment were analyzed before and 20 and 40 minutes after insulin administration. The samples were subjected to immunoprecipitation with anti-IRS-1 antibody and subsequently immunoblotted with antibodies as indicated. Experiments were performed in triplicate, and a representative picture is shown. (*A*) Immunoblot with antiphosphotyrosine antibody. There was no augmentation of phosphorylation of tyrosine in IRS-1 after insulin stimulation in the core gene transgenic mice, whereas tyrosine phosphorylation was markedly enhanced in control mice. Insulin-stimulated tyrosine phosphorylation was restored 40 minutes after anti-TNF-α antibody treatment. (*B*) Immunoblotting with anti-IRS-1 antibody as a control of IRS-1 load. nTg, nontransgenic mice; Tg, transgenic mice; anti-PY, antiphosphotyrosine antibody; anti-PS, antiphosphoserine antibody. IP, immunoprecipitation.

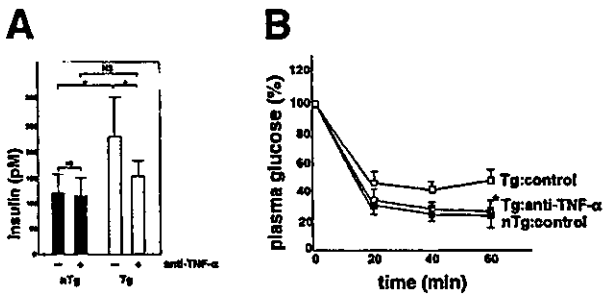

Figure 7. Serum insulin levels and insulin tolerance test after anti-TNF-α antibody treatment. (*A*) Serum insulin levels were determined in the fasting state with or without anti-TNF-α antibody treatment as described in the Materials and Methods section. Insulin levels decreased significantly after anti-TNF-α antibody treatment in the core gene transgenic mice (n = 5 in each group). (*B*) Insulin tolerance test (n = 5 in each group). Human insulin was administered by IP injection to fasted conscious mice and glucose concentrations were determined 24 hours after the second administration of anti-TNF-α antibody. As control, mice were injected with hamster IgG instead of anti-TNF-α antibody. Values were normalized to the baseline glucose concentration at the time of insulin administration. Values are mean ± standard error; $*P < 0.05$ when compared with Tg control; nTg, nontransgenic mice; Tg, transgenic mice.

The c-Jun N-terminal kinase (JNK) pathway has been shown to mediate the inhibitory effect of TNF-α on insulin action through the phosphorylation of serine in IRS-1.[32,33] Because an activation of the JNK pathway was observed in the liver of core gene transgenic mice,[13] phosphorylation of serine residues in IRS-1 was examined using antiphosphorylated serine monoclonal antibodies (Ser^{307} and Ser^{612}). However, there was no difference in the time course of serine phosphorylation after insulin stimulation between the core gene transgenic and control mice (data not shown).

Blockade of TNF-α Action Restores Insulin Sensitivity

Then the anti–TNF-α antibody was administered to block the in vivo activity of TNF-α in mice as described in the Materials and Methods section.[17] Twenty-four hours after the second administration of the anti–TNF-α antibody (200 μg/mouse), serum insulin levels in transgenic mice became significantly lower than the baseline (Figure 7*A*, 230.8 ± 70.7 vs. 153.6 ± 17.4 pmol/L, $P < 0.05$). Serum insulin levels in control mice also decreased, but there was no significant difference from the baseline (123.3 ± 36.1 vs. 112.0 ± 39.7 pmol/L, $P = 0.25$). Levels of FPG also decreased, but the difference from the baseline was not statistically significant. The insulin tolerance test conducted 24 hours after the second administration of anti–TNF-α antibody is shown in Figure 7*B*. As expected from serum insulin levels, anti–TNF-α antibody treatment restored the sen-

sitivity of the core gene transgenic mice to insulin activity. At this time point, phosphorylation of tyrosine in IRS-1 in the liver of transgenic mice in response to insulin action was restored to a similar level to that in control mice (Figure 6*A*, 40 minutes after insulin administration). These results strongly support the notion that the increased level of TNF-α is one of the bases for insulin resistance in the HCV core gene transgenic mice.

Taken together, these data indicate that the presence of the HCV core protein in the liver, at a level similar to that in human chronic hepatitis C patients,[21] confers insulin resistance to the mice by affecting the liver, by disturbing the insulin-induced suppression of hepatic glucose production.[34,35]

Discussion

Since Allison et al.[4] reported an association between HCV infection and diabetes, evidence has been accumulating connecting these 2 conditions. In such studies, HCV infection has a significantly stronger association with diabetes than hepatitis B viral infection.[4–7] The variables other than HCV infection that are associated with diabetes are cirrhosis, male sex,[5] and aging.[6] In addition to these clinic-based, case-control studies, Mehta et al.[7] have reported the result of investigation at population level. In this cross-sectional national survey, persons 40 years or older with HCV infection were more than 3 times more likely to have type 2 diabetes than those without HCV infection. Thus, the association of HCV infection with diabetes has become closer as shown by epidemiological studies. However, there are some difficulties in establishing a definite relationship between HCV infection and diabetes on the basis of epidemiological studies; in patients, there are other numerous factors perturbing the verification of the definite relationship, such as obesity, aging, or particularly advanced liver injuries. Moreover, the biological mechanism underlying diabetes or insulin resistance in HCV infection is unknown. In vitro or cultured cell studies have a very limited utility for the study of insulin resistance or diabetes because insulin resistance is a condition that involves multiple organs, such as the skeletal muscles and liver. Thus, the use of good experimental animal model systems may be useful both in establishing a definite relationship between diabetes and HCV infection and in elucidating the role of HCV in the development of insulin resistance.

In the current study, the HCV core gene transgenic mice exhibited insulin resistance as early as 1-month old, despite an apparent absence of glucose intolerance. Development of insulin resistance without any liver injury[10,11] or excessive body weight gain, as shown in the current study, clearly indicates that infection of HCV per se is a cause of the development of insulin resistance. Although only the core protein is expressed in these mice instead of HCV replication in humans, the fact that the intrahepatic core protein levels are similar between the core gene transgenic mice and chronic hepatitis C patients[20] warrants extrapolating the result into hepatitis C patients. Certainly, dispersion in the intrahepatic core protein levels in human chronic hepatitis C patients compared with the constant amount of the core protein must be taken into account. The occurrence of insulin resistance in the core gene transgenic mice as early as 1-month old also excluded the possibility that aging is a cause of insulin resistance. Nonetheless, aging could be an aggravating factor for insulin resistance. Thus, the current analysis shows a definite causal relationship between HCV infection and the development of insulin resistance.

Our earlier studies have shown the development of hepatic steatosis in these HCV core gene transgenic mice after the age of 3 months.[11] However, insulin resistance invariably preceded the occurrence of hepatic steatosis, indicating that insulin resistance is not a consequence of hepatic steatosis in these mice. Certainly, it is possible that insulin resistance in the core gene transgenic mice may be affected or aggravated after the occurrence of hepatic steatosis. On the other hand, insulin resistance may be one of the factors that cause hepatic steatosis,[19] whereas the impairment of very-low-density lipoprotein (VLDL) secretion from the liver and hypo-β-oxidation of fatty acids are considered to be the bases of development of hepatic steatosis in the core gene transgenic mice.[21,36]

The general mechanism underlying insulin resistance is not precisely understood and is considered to be multifactorial.[8,9,37,38] Chiefly, it involves glucose consumption by the skeletal muscle and glucose production in the liver. Our current analysis revealed a failure of insulin in the suppression of HPG in the liver and an absence of suppression of glucose uptake by the muscles in the core gene transgenic mice. Combined, these results indicate the insulin resistance in the core gene transgenic mice is chiefly due to hepatic insulin resistance. An elevated intrahepatic TNF-α level plays one of the roles in causing insulin resistance through suppressing insulin-induced tyrosine phosphorylation of IRS-1. It should be noted that TNF-α levels are invariably elevated in the sera of patients with HCV infection.[22] Moreover, restoration of insulin sensitivity after anti–TNF-α antibody administration strongly supports the notion that TNF-α

is, at least in this animal model, a major factor for the development of insulin resistance in HCV infection. Taken together, insulin resistance in the core gene transgenic mice mainly depends on suppression of the inhibitory effect of insulin on hepatic glucose production. This is consistent with the observation that the core protein is present only in the liver but absent in the skeletal muscle of the core gene transgenic mice (Tsutsumi T., unpublished data, December 2002).[21] Impairment in other undetermined pathways may also be responsible for the development of insulin resistance in HCV infection.

Insulin resistance alone does not always lead to the development of overt diabetes in humans or murine models. Particularly, in the models with the C57/BL6 strain,[18] hyperplasia of the islets of Langerhans in the pancreas compensates for insulin resistance by secreting higher amounts of insulin. Along with a gain in body weight by being fed a high-calorie diet, the core gene transgenic mice but no control mice developed overt diabetes, showing that obesity is a risk factor for diabetes as observed in patients or as shown in animal models for diabetes unrelated to HCV infection.[37,38] This observation would suggest that HCV infection confers insulin resistance and additional factors such as obesity, aging, or possibly inflammation may contribute to the complete development of overt diabetes. The effect of high-fat diet on control C57BL/6 mice may be milder in the current study compared with a previous study.[39] However, there was a substantial increase in FPG levels in high-fat-diet-fed control mice compared with normal-diet-fed control mice (Figures 1*B* and 4*B*). In addition, at fed-state, serum insulin levels in high-fat-diet-fed control mice were significantly increased compared with those in normal-diet-fed control mice (Figures 1*B* and 4*B*). It is unclear why plasma glucose levels were not very high at fed-state in control mice, but one possible explanation is the lower calorie content in the current study than those in the previous report: 4.70 kcal/g for our high-fat diet vs. 5.55 kcal/g for high-calorie diet in the previous study. A shorter duration of high-fat diet than the previous study (2 months vs. 6 months) may be another possible explanation.[39] Such a mild elevation in plasma glucose levels in high-fat-diet-fed C57BL/6 mice as the one observed in our study has also been described in previous studies.[40]

In conclusion, the HCV core protein induces insulin resistance in transgenic mice without gain in body weight at young age. These results indicate a direct involvement of HCV per se in the pathogenesis of diabetes in patients with HCV infection and provide a molecular basis for insulin resistance in such a condition.

References

1. Saito I, Miyamura T, Ohbayashi A, Harada H, Katayama T, Kikuchi S, Watanabe Y, Koi S, Onji M, Ohta Y, Choo Q, Houghton M, Kuo G. Hepatitis C virus infection is associated with the development of hepatocellular carcinoma. Proc Natl Acad Sci U S A 1990;87: 6547–6549.
2. Simonetti RG, Camma C, Fiorello F, Cottone M, Rapicetta M, Marino L, Fiorentino G, Craxi A, Ciccaglione A, Giuseppetti R, Stroffolini T, Pagliaro L. Hepatitis C virus infection as a risk factor for hepatocellular carcinoma in patients with cirrhosis. Ann Intern Med 1992;116:97–102.
3. Gumber SC, Chopra S. Hepatitis C: a multifaceted disease. Ann Intern Med 1995;123:615–620.
4. Allison ME, Wreghitt T, Palmer CR, Alexander GJ. Evidence for a link between hepatitis C virus infection and diabetes mellitus in a cirrhotic population. J Hepatol 1994;21:1135–1139.
5. Caronia S, Taylor K, Pagliaro L, Carr C, Palazzo U, Petrik J, O'Rahilly S, Shore S, Tom BD, Alexander GJ. Further evidence for an association between non-insulin-dependent diabetes mellitus and chronic hepatitis C virus infection. Hepatology 1999;30: 1059–1063.
6. Mason AL, Lau JY, Hoang N, Qian K, Alexander GJ, Xu L, Guo L, Jacob S, Regenstein FG, Zimmerman R, Everhart JE, Wasserfall C, Maclaren NK, Perrillo RP. Association of diabetes mellitus and chronic hepatitis C virus infection. Hepatology 1999;29:328–333.
7. Mehta SH, Brancati FL, Sulkowski MS, Strathdee SA, Szklo M, Thomas DL. Prevalence of type 2 diabetes mellitus among persons with hepatitis C virus infection in the United States. Ann Intern Med 2000;133:592–599.
8. Kahn BB. Type 2 diabetes: when insulin secretion fails to compensate for insulin resistance. Cell 1998;92:593–596.
9. Cavaghan MK, Ehrmann DA, Polonsky KS. Interactions between insulin resistance and insulin secretion in the development of glucose intolerance. J Clin Invest 2000;106:329–333.
10. Moriya K, Fujie H, Shintani Y, Yotsuyanagi H, Tsutsumi T, Matsuura Y, Kimura S, Miyamura T, Koike K. Hepatitis C virus core protein induces hepatocellular carcinoma in transgenic mice. Nat Med 1998;4:1065–1068.
11. Moriya K, Yotsuyanagi H, Shintani Y, Fujie H, Ishibashi K, Matsuura Y, Miyamura T, Koike K. Hepatitis C virus core protein induces hepatic steatosis in transgenic mice. J Gen Virol 1997; 78:1527–1531.
12. Koike K, Moriya K, Yotsuyanagi H, Shintani Y, Fujie H, Ishibashi K, Matsuura Y, Kurokawa K, Miyamura T. Sialadenitis resembling Sjögren's syndrome in mice transgenic for hepatitis C virus envelope genes. Proc Natl Acad Sci U S A 1997;94:233–236.
13. Tsutsumi T, Suzuki T, Moriya K, Yotsuyanagi H, Shintani Y, Fujie H, Matsuura Y, Kimura S, Koike K, Miyamura T. Intrahepatic cytokine expression and AP-1 activation in mice transgenic for hepatitis C virus core protein. Virology 2002;304:415–424.
14. Fujie H, Moriya K, Shintani Y, Tsutsumi T, Takayama T, Makuuchi M, Kimura S, Koike K. Frequent β-catenin aberration in human hepatocellular carcinoma. Hepatol Res 2001;20:39–51.
15. Ren JM, Marshall BA, Mueckler MM, McCaleb M, Amatruda JM, Shulman GI. Overexpression of Glut4 protein in muscle increases basal and insulin-stimulated whole body glucose disposal in conscious mice. J Clin Invest 1995;95:429–432.
16. Brozinick T Jr, Birnbaum MJ. Insulin, but not contraction, activates Akt/PKB in isolated rat skeletal muscle. J Biol Chem 1998;273:14679–14682.
17. Williams RO, Marinova-Mutafchieva L, Feldmann M, Maini RN. Evaluation of TNF-alpha and IL-1 blockade in collagen-induced arthritis and comparison with combined anti-TNF-alpha/anti-CD4 therapy. J Immunol 2000;165:7240–7245.
18. Polonsky KS, Sturis J, Bell GI. Seminars in medicine of the Beth

Israel Hospital, Boston. Non-insulin-dependent diabetes mellitus—a genetically programmed failure of the beta cell to compensate for insulin resistance. N Engl J Med 1996;334:777–783.
19. Chatila R, West AB. Hepatomegaly and abnormal liver tests due to glycogenosis in adults with diabetes. Medicine (Baltimore) 1996;75:327–333.
20. Koike K, Moriya K, Ishibashi K, Matsuura Y, Suzuki T, Saito I, Iino S, Kurokawa K, Miyamura T. Expression of hepatitis C virus envelope proteins in transgenic mice. J Gen Virol 1995;76:3031–3038.
21. Koike K, Tsutsumi T, Fujie H, Shintani Y, Moriya K. Role of hepatitis viruses in hepatocarcinogenesis. Oncology 2002;62: 29–37.
22. Polyak SJ, Khabar KS, Rezeiq M, Gretch DR. Elevated levels of interleukin-8 in serum are associated with hepatitis C virus infection and resistance to interferon therapy. J Virol 2001;75:6209–6211.
23. Kallinowski B, Haseroth K, Marinos G, Hanck C, Stremmel W, Theilmann L, Singer MV, Rossol S. Induction of tumour necrosis factor (TNF) receptor type p55 and p75 in patients with chronic hepatitis C virus (HCV) infection. Clin Exp Immunol 1998;111: 269–277.
24. Nelson DR, Lim HL, Marousis CG, Fang JW, Davis GL, Shen L, Urdea MS, Kolberg JA, Lau JY. Activation of tumor necrosis factor-alpha system in chronic hepatitis C virus infection. Dig Dis Sci 1997;42:2487–2494.
25. Gershon AS, Margulies M, Gorczynski RM, Heathcote EJ. Serum cytokine values and fatigue in chronic hepatitis C infection. J Viral Hepat 2000;7:397–402.
26. Moller DE. Potential role of TNF-alpha in the pathogenesis of insulin resistance and type 2 diabetes. Trends Endocrinol Metab 2000;11:212–217.
27. Halse R, Pearson SL, McCormack JG, Yeaman SJ, Taylor R. Effects of tumor necrosis factor-alpha on insulin action in cultured human muscle cells. Diabetes 2001;50:1102–1109.
28. Mishima Y, Kuyama A, Tada A, Takahashi K, Ishioka T, Kibata M. Relationship between serum tumor necrosis factor-alpha and insulin resistance in obese men with type 2 diabetes mellitus. Diabetes Res Clin Pract 2001;52:119–123.
29. Uysal KT, Wiesbrock SM, Marino MW, Hotamisligil GS. Protection from obesity-induced insulin resistance in mice lacking TNF-alpha function. Nature 1997;389:610–614.
30. Hotamisligil GS. The role of TNF alpha and TNF receptors in obesity and insulin resistance. J Intern Med 1999;245:621–625.
31. Ozes ON, Akca H, Mayo LD, Gustin JA, Maehama T, Dixon JE, Donner DB. A phosphatidylinositol 3-kinase/Akt/mTOR pathway mediates and PTEN antagonizes tumor necrosis factor inhibition of insulin signaling through insulin receptor substrate-1. Proc Natl Acad Sci U S A 2001;98:4640–4645.
32. Aguirre V, Uchida T, Yenush L, Davis R, White MF. The c-Jun NH(2)-terminal kinase promotes insulin resistance during association with insulin receptor substrate-1 and phosphorylation of Ser(307). J Biol Chem 2000;275:9047–9054.
33. De Fea K, Roth RA. Protein kinase C modulation of insulin receptor substrate-1 tyrosine phosphorylation requires serine 612. Biochemistry 1997;36:12939–12947.
34. Michael MD, Kulkarni RN, Postic C, Previs SF, Shulman GI, Magnuson MA, Kahn CR. Loss of insulin signaling in hepatocytes leads to severe insulin resistance and progressive hepatic dysfunction. Mol Cell 2000;6:87–97.
35. Cho H, Mu J, Kim JK, Thorvaldsen JL, Chu Q, Crenshaw EB 3rd, Kaestner KH, Bartolomei MS, Shulman GI, Birnbaum MJ. Insulin resistance and a diabetes mellitus-like syndrome in mice lacking the protein kinase Akt2 (PKB beta). Science 2001;292:1728–1731.
36. Perlemuter G, Sabile A, Letteron P, Topilco Samson-Bouna M-E, Chretien Y, Pessayre D, Koike K, Chapman J, Barba G, Brechot C. Hepatitis C virus core protein inhibits microsomal triglyceride transfer protein activity and very low density lipoprotein secretion: a model of viral-related steatosis. FASEB J 2002;16:185–194.
37. Kahn BB, Flier JS. Obesity and insulin resistance. J Clin Invest 2000;206:473–481.
38. Kadowaki T. Insight into insulin resistance and type 2 diabetes from knockout mouse models. J Clin Invest 2000;206:459–465.
39. Surwit RS, Feinglos MN, Rodin J, Sutherland A, Petro AE, Opara EC, Kuhn CM, Rebuffe-Scrive M. Differential effects of fat and sucrose on the development of obesity and diabetes in C57BL/6J and A/J mice. Metabolism 1995;44:645–651.
40. Devedjian JC, George M, Casellas A, Pujol A, Visa J, Pelegrin M, Gros L, Bosch F. Transgenic mice overexpressing insulin-like growth factor-II in beta cells develop type 2 diabetes. J Clin Invest 2000;105:731–740.

Received May 30, 2003. Accepted November 20, 2003.

Address requests for reprints to: Kazuhiko Koike, M.D., Department of Infectious Diseases, Internal Medicine, Graduate School of Medicine, University of Tokyo, 7-3-1 Hongo, Bunkyo-ku, Tokyo 113-8655, Japan. e-mail: kkoike-tky@umin.ac.jp; fax: (81) 3-5800-8807.

Supported by a grant-in-aid for Scientific Research on Priority Area from the Ministry of Education, Science, Sports and Culture of Japan; Health Sciences Research Grants of The Ministry of Health, Welfare and Labor; The Program for Promotion of Fundamental Studies in Health Sciences of the Organization for Drug ADR Relief, R&D Promotion and Product Review of Japan; and grant from The Sankyo Foundation of Life Science.

Y.S. and H.F. contributed equally to this work.

Despite their results, even if they seem strongly suggest an important role for TNF-α, is our opinion that the responsibility of this cytokine should be considered carefully.

In our previous study (Int J Immunopathol and Pharmacol [in press]) we assayed the TNF-α serum levels in patients with and without DM during CHC, not finding any statistical significant differences in its concentrations. In our groups, all the patients did not present obesity or hypertrigliceridemia or else hypercholesterolemia.

Taking into consideration that insulin resistance and DM type 2 are correlated to peripheral alteration of glucose metabolism TNF related[7] and on the light of the authors evidences on transgenic mice model how we could take to mean our results?

These evidences taken together seem suggest the presence of 2 different network in CHC; hepatic and peripheral.

In the liver the likely source of TNF-α production should be the Kupffer cells,[8] so have the authors evaluated these cells at a liver biopsy or TNF-α concentrations in serum?

Otherwise, how they explain the increased levels found, considering also that the transgenic mice do not present the same inflammation of an HCV infected patient?

The significance of TNF-α augmented serum levels during CHC natural history, and its possible effects on metabolism seem to be not so clear. Consequently, considering that other cytokines are been suggested in diabetes mellitus as IL-6[9]; how we can judge as guilty the TNF-α?

Moreover, making an allowance for the infective and immune adverse effects,[10] which should be the rational of an eventual anti-TNF treatment in infected patients?

In conclusion, although the interesting work of Shintani et al., on transgenic mice, focuses new attention on HCV direct role on insulin resistance, the fascinating connection with a possible cytokine environments in this metabolic disorder is really still unclear. A wider cytokine network evaluation both in liver and periphery is required to understand the intricate inflammatory network in DM pathogenesis in humans during chronic hepatitis C.

ALESSANDRO PERRELLA
GUGLIELMO BORGIA
LAURA REYNAUD
FRANCESCO BORRELLI
SILVANA DI SIRIO
STELLA GRATTACASO
Department of Infectious Disease and Public Health
Federico II Medical School University
Naples, Italy

ORESTE PERRELLA
VII Department of Infectious Disease and Immunology
Hospital D.Cotugno
Naples, Italy

1. Marchesini G, Brizi M, Bianchi G, Tomassetti S, Bugianesi E, Lenzi M, McCullough AJ, Natale S, Forlani G, Melchionda N. Nonalcoholic fatty liver disease: a feature of the metabolic syndrome. Diabetes 2001;50:1844–1850.
2. Aytug S, Reich D, Sapiro LE, Bernstein D, Begum N. Impaired IRS-1/PI3-kinase signaling in patients with HCV: a mechanism for increased prevalence of type 2 diabetes. Hepatology 2003;38: 1384–1392.
3. Knobler H, Zhornicky T, Sandler A, Haran N, Ashur Y, Schattner A. Tumor necrosis factor-α-induced insulin resistance may mediate the hepatitis C virus-diabetes association. Am J Gastroenterol 2003;98:2751–2756.
4. Hotamisligil GS. The role of TNF-α and TNF receptors in obesity and insulin resistance. J Intern Med 1999;245:621–625.
5. Shintani Y, Fujie H, Miyoshi H, Tsutsumi T, Tsukamoto K, Kimura S, Moriya K, Koike K. Hepatitis C virus infection and diabetes: direct involvement of the virus in the development of insulin resistance. Gastroenterology 2004;126:840.
6. Nelson DR, Lim HL, Marousis CG, Fang JW, Davis GL, Shen L, Urdea MS, Kolberg JA, Lau JY. Activation of tumor necrosis factor-alpha system in chronic hepatitis C virus infection. Dig Dis Sci 1997;42:2487.
7. Hotamisligil GS. The role of TNF-α and TNF receptors in obesity and insulin resistance. J Intern Med 1999;245:621–625.
8. Dong W, Simeonova PP, Gallucci R, Matheson J, Fannin R, Montuschi P, Flood L, Luster MI. Cytokine expression in hepatocytes: role of oxidant stress. J Interferon Cytokine Res 1998;18:629–638.
9. Klover PJ, Zimmers TA, Koniaris LG, Mooney RA. Chronic exposure to interleukin-6 causes hepatic insulin resistance in mice. Diabetes 2003;52:2784–2789.
10. Gomez-Reino JJ, Carmona L, Valverde VR, Mola EM, Montero MD, BIOBADASER Group. Treatment of rheumatoid arthritis with tumor necrosis factor inhibitors may predispose to significant increase in tuberculosis risk: a multicenter active-surveillance report. Arthritis Rheum 2003;48:2122–2127.

doi:10.1053/j.gastro.2004.08.059

Reply. We appreciate the comments of Perrella et al.[1] on our recent study published in GASTROENTEROLOGY. We realized afresh that the association of diabetes and hepatitis C virus (HCV) infection is a major concern to gastroenterologists and researchers in related fields. We also appreciate their comment that our study has focused a new attention on the direct role of HCV on insulin resistance. Their key point is that it is not clear yet whether TNF-α is a central mediator for insulin resistance in chronic HCV infection according to their data and the considerations on the cytokine network.

We agree to their comment in the point that we should be careful in assessing the role of TNF-α in the genesis of insulin resistance in HCV infection, in particular, in human patients, where numerous other factors than those in an animal model would play roles in glucose homeostasis. In our article, we have stated that the increased level of TNF-α is one of the bases for insulin resistance in the mouse model but impairment in other undetermined pathways may also be responsible for the development of insulin resistance in HCV infection.[1] Insulin resistance in our mouse model is chiefly the central one, i.e., derived from the liver; suppression of insulin action on the hepatic glucose production is inhibited. Considering this specific involvement of the liver, the levels of TNF-α not in the serum but in the liver would be essential in development of insulin resistance in this mouse model. Unfortunately, we cannot access the data by Perrella et al. that there was no significant difference in serum TNF-α levels between the hepatitis C patients with and without diabetes, but we suppose the number of patients analyzed was large enough to verify the absence of difference. Nonetheless, the levels of TNF-α in the liver, where HCV replicates, may be critical in development of the central insulin resistance.

Naturally, it is possible that the core protein operates directly to inhibit insulin action of tyrosine-phosphorylation of insulin receptor sustrate-1,[1] which inhibition was, interestingly, also observed in the liver of chronic hepatitis C patients.[2] On the other hand, because the expression of the core protein was virtually limited to the liver in the mice,[3] the contribution of peripheral factor to insulin resistance,[4] which may be present in human hepatitis C patients, could not be evaluated in our study. Mitochondrial dysfunction, suggested to have

a role in insulin resistance in the elderly,[5] might also have a contribution in insulin resistance in HCV infection.

In our mouse model, we have not identified the type of cells that produce TNF-α in the liver, but determination of other cytokines including IL-6 was already done: only TNF-α and IL-1β levels were increased in the liver among numerous cytokines.[6] Serum levels of TNF-α were determined as well, resulting to be below the detection limit of sensitive Elisa assays (Moriya K, et al. unpublished data). As described previously, there was no histopathological inflammation in the liver of HCV core gene transgenic mice.[3] However, such increases in intrahepatic proinflammatory cytokine levels, combined with the overproduction of reactive oxygen species (ROS),[7] allow us to hypothesize that HCV core protein *per se* induces "biochemical inflammation" in the mouse liver in the absence of apparent inflammation.

In summary, from our data, an impairment of intracellular insulin signaling pathway in the liver is the basis for insulin resistance in HCV infection, in which an elevated intrahepatic TNF-α level would be one of the key factors. Additional factors associated with insulin resistance must be explored, in particular, associated with peripheral insulin resistance.

KAZUHIKO KOIKE, M.D., Ph.D.
HAJIME FUJIE, M.D.
YOSHIZUMI SHINTANI, M.D.
HIDEYUKI MIYOSHI, M.D.
KYOJI MORIYA, M.D., Ph.D.
Department of Internal Medicine
Graduate School of Medicine
University of Tokyo
Tokyo, Japan

1. Shintani Y, Fujie H, Miyoshi H, Tsutsumi T, Kimura S, Moriya K, Koike K. Hepatitis C virus and diabetes: direct involvement of the virus in the development of insulin resistance. Gastroenterology 2004;126:840–848.
2. Aytug S, Reich D, Sapiro LE, Bernstein D, Begum N. Impaired IRS-1/PI3-kinase signaling in patients with HCV: a mechanism for increased prevalence of type 2 diabetes. Hepatology 2003;38: 1384–1392.
3. Moriya K, Fujie H, Shintani Y, Yotsuyanagi H, Tsutsumi T, Matsuura Y, Kimura S, Miyamura T, Koike K. Hepatitis C virus core protein induces hepatocellular carcinoma in transgenic mice. Nat Med 1998;4:1065–1068.
4. Kadowaki T. Insight into insulin resistance and type 2 diabetes from knockout mouse models. J Clin Invest 2000;206:459–465.
5. Petersen KF, Befroy D, Dufour S, Dziura J, Ariyan C, Rothman DL, DiPietro L, Cline GW, Shulman GI. Mitochondrial dysfunction in the elderly: possible role in insulin resistance. Science 2003;300: 1140–1142.
6. Tsutsumi T, Suzuki T, Moriya K, Yotsuyanagi H, Shintani Y, Fujie H, Matsuura Y, Kimura S, Koike K, Miyamura T. Intrahepatic cytokine expression and AP-1 activation in mice transgenic for hepatitis C virus core protein. Virology 2002;304:415–424.
7. Moriya K, Nakagawa K, Santa T, Shintani Y, Fujie H, Miyoshi H, Tsutsumi T, Miyazawa T, Ishibashi K, Horie T, Imai K, Miyamura T, Kimura S, Koike K. Oxidative stress in the absence of inflammation in a mouse model for hepatitis C virus-associated hepatocellular carcinogenesis. Cancer Res 2001;61:4365–4370.

doi:10.1053/j.gastro.2004.08.060

Available online at www.sciencedirect.com
SCIENCE DIRECT®
Biochemical and Biophysical Research Communications 325 (2004) 1131–1135
BBRC
www.elsevier.com/locate/ybbrc

Tumor size-independence of telomere length indicates an aggressive feature of HCC☆

Tomoki Nakajima[a,*], Tatsuo Katagishi[a], Michihisa Moriguchi[a], Satoru Sekoguchi[a], Taichirou Nishikawa[a], Hidetaka Takashima[a], Tadashi Watanabe[a], Hiroyuki Kimura[a], Masahito Minami[a], Yoshito Itoh[a], Keizo Kagawa[b], Takeshi Okanoue[a]

[a] *Molecular Gastroenterology and Hepatology, Kyoto Prefectural University of Medicine Graduate School of Medical Science, Kawaramachi-Hirokoji, Kamigyo-ku, Kyoto 602-8566, Japan*
[b] *Department of Medicine, Fukuchiyama City Hospital, Atsunaka-cho, Fukuchiyama, Kyoto, Japan*

Received 17 September 2004
Available online 11 November 2004

Abstract

Using quantitative fluorescence in situ hybridization (Q-FISH), the average telomere length of hepatoma cells was assessed by the average telomeric signal intensity of cancer cells relative to that of stromal cells. We demonstrated first the applicability of Q-FISH for tissue sections by comparing Q-FISH and Southern blotting results. Tumors less than 50 mm in diameter and with a relative telomeric intensity of less than 0.6 were categorized as group A and the remainder as group B. In group A, the telomere length correlated negatively with tumor size, whereas in group B there was no correlation. Compared with the group A tumors, the group B tumors were of significantly more advanced stage, showed higher telomerase and proliferative activities, and exhibited less differentiated histology. Therefore, we considered that a lack of correlation between telomere length and tumor size, namely, size-independence of telomere length, is associated with unfavorable clinicopathological features of hepatocellular carcinomas.
© 2004 Elsevier Inc. All rights reserved.

Keywords: Hepatocellular carcinoma; Quantitative fluorescence in situ hybridization; Telomere length; Tumor size

The telomeres at the ends of chromosomes are composed of terminal DNA sequence repeats and telomere-binding proteins [1]. These structures have an essential role in the maintenance of chromosomal stability by capping the chromosomes and protecting them from end-to-end fusion. Telomere repeat sequences are subjected to shortening with each cell division because of their incomplete replication during DNA synthesis [2]. The loss of telomere repeat sequences has been proposed as a possible mechanism of cellular senescence [1,3]. Conversely, in germ cells, the majority of established cell lines, and more than 85% of malignant cells, the length of the telomeres is maintained or increased through the action of telomerase [4].

The average length of telomeres is assessed conventionally by Southern blot analysis. However, this method has several drawbacks [5–8]. First, more than 10^5 cells are needed to obtain sufficient DNA. Second, the restriction enzyme used to prepare the DNA cleaves at sites in the subtelomeric DNA at various distances from the beginning of the repetitive sequences and, therefore, the terminal restriction fragments (TRFs) measured by Southern blot analysis include the telomeres and subtelomeric sequences of unknown length. Third, this method provides no information regarding the telomere lengths in individual cells. The last problem is particularly important when investigating tissues

☆ *Abbreviations:* HCC, hepatocellular carcinoma; Q-FISH, quantitative fluorescence in situ hybridization.

* Corresponding author. Fax: +81 75 251 0710.
E-mail address: tomnaka@silver.ocn.ne.jp (T. Nakajima).

0006-291X/$ - see front matter © 2004 Elsevier Inc. All rights reserved.
doi:10.1016/j.bbrc.2004.10.152

comprising several types of parenchymal and stromal cells with different telomere lengths.

Approximately 60% of the normal liver consists of hepatocytes. The remainder includes biliary epithelia, sinusoidal cells (endothelial cells, Kupffer cells, hepatic stellate cells, and pit cells), and infiltrating blood cells. During chronic liver cell injury, the telomere sequences of hepatocytes are shortened progressively, but those of other cells, particularly infiltrating lymphocytes, are shortened to a lesser degree, because of their weak telomerase activity [9,10]. Southern blotting, therefore, may provide misleading results from DNA extracted from a mixture of several types of cells in the liver.

Quantitative fluorescence in situ hybridization (Q-FISH) using a telomere-specific probe enabled us to assess telomere lengths at the level of the individual cell [5–8]. In this study, we determined first whether this method can be applied to paraffin-embedded tissue sections of diseased liver by comparing the results of Q-FISH with those of Southern blotting. Then, we elucidated the biological significance of telomere lengths in hepatocellular carcinoma (HCC) in terms of clinicopathological parameters.

Materials and methods

Patients. Liver tissues containing HCC were obtained from 14 male and 16 female patients at surgery. The patients were 60.5 ± 9.3 years old and none had received preoperative chemotherapeutic or interventional treatment. Five patients were serologically positive for hepatitis B surface antigen (HBsAg) only, 23 for anti-hepatitis C antibody (anti-HCV) only, one was positive for both HBsAg and anti-HCV, and one was negative for both HBsAg and anti-HCV. Two patients were in stage I, 20 were in stage II, 6 were in stage III, and 2 were in stage IV according to the TNM classification. Nine tumors were of the well-differentiated type, 11 were of the moderately differentiated type, and 10 were of the poorly differentiated type. Controls for this study were histologically normal liver tissues from two patients who underwent partial hepatectomy for metastatic liver cancers. Informed consent was obtained from all patients in a written form.

Sample preparation. A portion of each sample was immediately frozen with liquid nitrogen and stored at −80 °C before use for the telomere repeat amplification protocol (TRAP) assay [11] and Southern blot analysis [12]. The remainder was fixed with 4% buffered paraformaldehyde at 4 °C overnight and paraffin-embedded for histological examination. Sections were cut from the faces of the frozen tissue blocks immediately adjacent to the faces of the matching paraffin blocks, from which sections had been cut previously for histological assessment. Two frozen sections of an average thickness of 20 μm were cut from each tissue block and used for protein and DNA extraction.

Three sections of 5 μm-thickness were cut serially from each paraffin block. These were used for quantitative fluorescence in situ hybridization (Q-FISH) for the telomere region, hematoxylin and eosin (HE) staining, and immunohistochemical staining for Ki-67 antigen. Tumor histological grades were determined according to the classification of the Liver Cancer Study Group of Japan [13].

Evaluation of telomere length by Southern blot analysis. DNA was purified from the samples by digestion with proteinase K and phenol–chloroform extraction. Ten micrograms of DNA was digested overnight with 6 U/μg of the restriction endonuclease *Hin*fI (Takara, Japan) at 37 °C. The terminal restriction fragments (TRFs) were separated by electrophoresis on a 0.8% agarose gel at 2.5 V/cm for 20 h, depurinated in 0.25 N HCl, and denatured in 1.5 M NaCl containing 0.5 M NaOH. Then, the DNA fragments were transferred to a nylon membrane (Hybond N+, Amersham, Buckinghamshire, UK) by capillary blotting. An oligonucleotide $(TTAGGG)_4$ was used as the probe and was labelled with fluorescein-dUTP using an ECL 3′-oligolabeling kit (Amersham). After prehybridization for 30 min, hybridization was performed at 45 °C in 5× SSC containing 0.5% blocking agent (provided in the kit), 0.02% SDS and 0.5% hybridization buffer component (provided in the kit) in a hybridization oven (KURABO, Japan) for 17 h. After washes with 1× SSC containing 0.1% SDS at 50 °C for 30 min, hybridized probes were detected by chemiluminescence using an ECL detection system (Amersham) according to the manufacturer's protocol and exposed to X-ray films for 15 min. For densitometric analysis, after the image was captured by a CCD camera, the size of the mean TRF was determined as the indicator of mean telomere length at the peak position of the hybridization signals, using ATTO densitograph software (version 4.02, ATTO, Japan).

Semiquantitative analysis of telomerase activity by TRAP assay. The TRAP assay was performed using a TRAPEZE Telomerase Detection Kit (Oncor, Gaithersburg) according to the manufacturer's protocol. Six micrograms of protein was assayed in 50 μl of reaction mixture composed of reaction buffer (20 mM Tris–HCl, pH 8.3, 1.5 mM $MgCl_2$, 63 mM KCl, 0.05% Tween 20, 1 mM EGTA, and 0.01% bovine serum albumin), 50 mM of each deoxynucleotide triphosphate, 0.1 μg TS primer (5′-AATCCGTCGAGCAGAGTT-3′), and 2 U *Taq* DNA polymerase (Takara, Japan). After a 30-min incubation at 30 °C, the mixture was incubated for 5 min at 90 °C to inactivate the telomerase. Then, the samples were subjected to 30 PCR cycles at 94 °C for 30 s, 52 °C for 30 s, and 72 °C for 60 s (final extension 120 s). Twenty microliters of PCR product was loaded and run on a 12% non-denaturing polyacrylamide gel in 0.5× Tris–borate–EDTA buffer. After electrophoresis, the gel was stained with SYBR Green 1 (Molecular Probes, Eugene, USA) for 30 min.

Evaluation of telomerase activity was carried out using a CCD imaging system (ATTO) and ATTO densitograph software. To control the telomerase activity of the six-nucleotide ladder, protein extracts were incubated at 85 °C for 10 min prior to mixing with the reaction mixture (heat-inactivated control). Internal control oligonucleotides K1 and TSK1 which, together with the TS primer, produce a 36 bp band, were used to distinguish false negative results attributable to the presence of intrinsic inhibitors of *Taq* polymerase in the extracts. For semiquantitative analysis, a TSR8 control template was used instead of the sample extract (quantitation control). TSR8 is an oligonucleotide with a sequence identical to the TS primer extended with eight telomeric repeats. This control serves as a standard for estimating the amount of TS primers with telomeric repeats extended by telomerase in a given extract. The relative telomerase activity in a sample was derived from the ratio of the intensity between the internal control and the telomerase ladder in a lane using the following formula:

$$\mathrm{RTA} = 100 \times \{(X/C)/(r/CR)\},$$

where RTA is the relative telomerase activity, X is the signal of the region of the gel corresponding to the TRAP product ladder bands from the sample, and C is from the internal standard in each sample. Similarly, r and CR are the signals from the TSR8 quantification control lane and internal control lane, respectively. Telomerase activities were classified into the following three groups: $1+ (0 < \mathrm{RTA} < 50)$, $2+ (50 \leqq \mathrm{RTA} < 100)$, and $3+ (100 \leqq \mathrm{RTA})$.

Quantitative fluorescence in situ hybridization for telomere length. The telomere length of each cell was assessed by measuring the fluorescent intensity of telomere FISH on each paraffin section. Paraffin sections were deparaffinized with xylene, hydrated through a graded

ethanol series, and then placed in deionized water (DW). Slides were then autoclaved at 121 °C for 20 min in Target Retrieval Solution (Catalog No. S1700; DAKO, Kyoto). After cooling to room temperature for 20 min, the slides were washed in DW for 1 min three times, and immersed in 0.3% hydrogen peroxide/absolute methanol at room temperature for 20 min to block endogenous peroxidase. Slides were placed in DW for 3 × 2 min, in 70% ethanol for 1 min, in 95% ethanol for 1 min, in 100% ethanol for 1 min, and then air-dried. Ten microliters of a fluorescent isothiocyanate (FITC)-labelled telomere-specific peptide nucleic acid (PNA) probe (vial 2 in K 5325, DAKO, Denmark) was applied to each sample, which was then covered with an 18 × 18 mm coverslip, and denatured on a heat block at 90 °C for 5 min. Slides were then moved to a dark moisture chamber at 45 °C overnight. Coverslips were then carefully removed in Tris-buffered saline with Tween 20 (TBST) (Item No. 003178 in K0618, DAKO, Denmark) and the slides were washed in wash solution (vial 4 in K 5325) at a dilution of 1:50 at 52 °C for 20 min, followed by 5 × 3-min washes in TBST. The slides were incubated with anti-FITC-horseradish peroxidase (HRP) (Item No. 004404 in K0618) diluted 1:100 in anti-FITC-HRP diluent (Item No. 004407 in K0618) at room temperature for 30 min, followed by 5 × 3-min washes in TBST. Seventy microliters of Fluorescyl Tyramide (Item No. 004409 in K0618) was applied to each slide at room temperature for 15 min. The slides were then immersed in TBST for 5 × 3 min, counterstained with 4′-6-diamidino-2-phenylindole (DAPI) (1000 ng/ml, VYS-32-804830, Vysis), and finally coverslipped.

Fluorescent microscopy and image analysis of telomeres. Following the protocol of Meeker et al. [5], image-processed telomeric signals were quantified from digitized fluorescence microscopic images using the image analysis software package IP Labs (version 3.54, Scanalytics, Fairfax, VA). Non-lymphocyte stromal cells were used as internal controls, following previous reports [14–16]. The resulting sums of telomeric pixel intensities for 15–20 nuclei of cancer cells and those of non-lymphocyte stromal cells were recorded. To control for different amounts of DNA in the sectioned nuclei, telomeric signal intensity was modified by dividing each telomere fluorescence sum for a given nucleus by the sum of the pixels of the DAPI signal within that nucleus, as reported previously [5]. The average modified telomeric signal intensity of cancer cells and that of non-lymphocyte stromal cells were designated as Tel-T and Tel-S, respectively. We assessed the ratio Tel-T/Tel-S as relative telomere length under various histological conditions.

Results

In normal liver tissues, strong telomeric signals were observed in the stromal cells. The telomeric signal intensities of cancer cells were mostly weaker than those of the non-lymphocyte stromal cells (Fig. 1A).

First in this study, the telomere lengths were assessed by Southern blotting and by Q-FISH (Fig. 1B). A significant correlation was noted between TRF assessed by Southern blotting and the relative signal intensity (Tel-T/Tel-S) by Q-FISH (Fig. 2A, $r = 0.651$, $p < 0.0001$, $n = 30$). Therefore, we concluded that Q-FISH was applicable to paraffin-embedded liver tissues under our conditions.

The telomere signal intensities of cancer cells relative to those of the stromal cells (Tel-T/Tel-S ratio) ranged from 0.11 to 1.33. In eight tumors, this ratio was larger 0.6 and relative telomere intensities were not correlated with tumor size (indicated by triangles in Fig. 2B). In the remaining 22 tumors, Tel-T/Tel-S ratio was less than 0.6. The relative telomere intensities of these tumors were correlated with tumor size before the tumor size reached 50 mm (indicated by closed circles in Fig. 2B and shown separately in Fig. 2C, ($r = 0.460, p < 0.05, n = 18$). However, when the tumors were 50 mm or larger, the relative telomere intensities were higher than expected for the tumor size ($n = 4$, indicated by open circles in Fig. 2B).

The tumors whose relative telomere lengths were correlated negatively with tumor size were categorized as group A (indicated by closed circles in Fig. 2B, $n = 18$) and the remaining tumors, which showed no relationship between tumor size and relative telomere length, were categorized as group B (indicated by triangles and open circles in Fig. 2B, $n = 12$). Compared with the group A tumors, the group B tumors were significantly more likely to be of

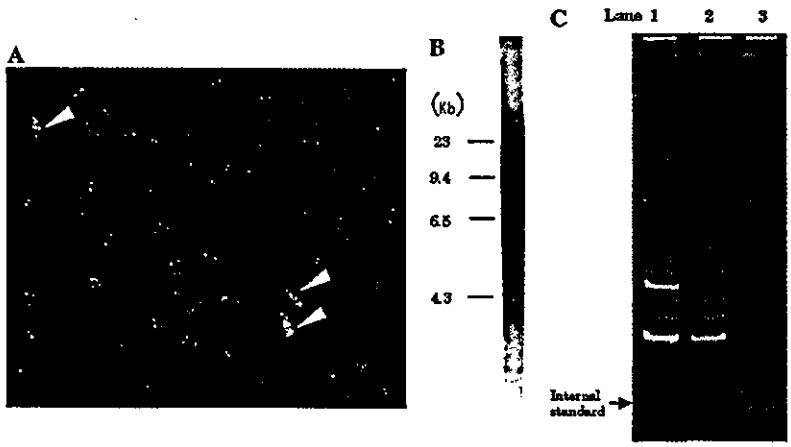

Fig. 1. (A) Representative telomere FISH in hepatocellular carcinoma (HCC). Stromal cells are indicated by arrowheads. (B) Representative results of telomere length analyzed by Southern blotting. (C) Representative examples of telomere repeat amplification protocol assay in the same tumor as (B). Lanes 1 and 3 show the quantitation control and the heat-inactivated (85 °C, 10 min) control, respectively. The band at the bottom of each lane represents the internal standard.

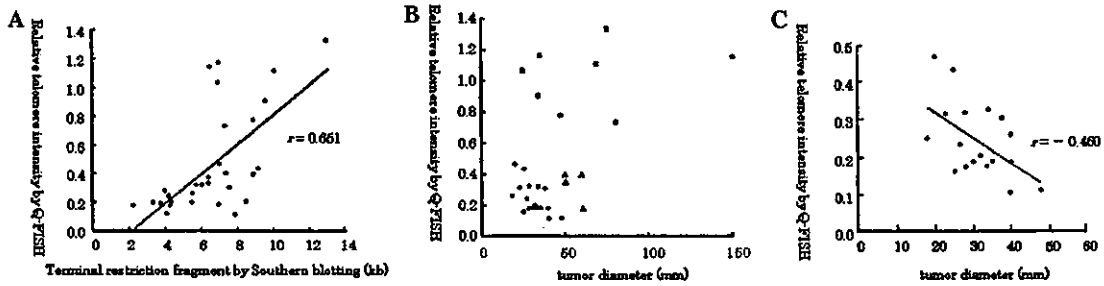

Fig. 2. (A) A significant correlation was noted between the terminal restriction fragment assessed by Southern blotting and the relative signal intensity (the average telomeric signal of cancer cells divided by the average telomeric signal of corresponding non-lymphocyte stromal cells) by quantitative FISH ($r = 0.504$, $p < 0.01$, $n = 30$). (B) The telomere signal intensities of cancer cells relative to non-lymphocyte stromal cells ranged from 0.11 to 1.33. In eight tumors (open circles) this ratio was larger than 0.6. Of the remaining 22 tumors, 18 were less than 50 mm in size (closed circles) and four were 50 mm or larger (closed triangles). (C) In the tumors whose relative telomeric intensities were less than 0.6 and whose sizes were less than 50 mm in diameter (closed circles in (B), the telomeric intensities were negatively correlated with tumor size ($r = -0.460$, $p < 0.05$, $n = 18$).

Table 1
The tumors whose telomere lengths correlated negatively with tumor size were categorized as group A and the remaining tumors, which showed no relationship between tumor size and telomere length, were categorized as group B

	Group A	Group B	
TNM stage			$p = 0.0342$
I + II	16	6	
III+IV	2	6	
Telomerase activity			$p = 0.0110$
—	4	0	
1+	10	4	
2+	3	6	
3+	1	2	
Histological grade			$p = 0.0492$
Well	8	1	
Moderately + poorly	10	11	
Proliferative activity			$p = 0.0188$
Ki positive Index (%)	16.6 ± 7.5	22.8 ± 8.1	

Compared with the group A tumors, group B tumors shows significantly higher incidence of stage III or IV ($p = 0.0342$ by Fisher's exact probability test), higher telomerase activity ($p = 0.0110$ by Mann–Whitney U test), higher proliferative activity ($p = 0.0188$ by Mann–Whitney U test), and higher incidence of moderately or poorly differentiated histology ($p = 0.0492$ by Fisher's exact probability test), and a higher proliferative activity ($p = 0.0188$ by Mann–Whitney U test).

stage III or IV ($p = 0.0342$ by Mann–Whitney U test) and have higher telomerase activity ($p = 0.0110$ by Mann–Whitney U test), a higher incidence of moderately or poorly differentiated histology ($p = 0.0492$ by Fisher's exact probability test), and a higher proliferative activity ($p = 0.0188$ by Mann–Whitney U test) (Table 1).

Discussion

One previous study using cell lines demonstrated that the average TRF values assessed by Southern blotting are significantly related to the telomere lengths measured by Q-FISH after paraffin-embedding [5]. Using paraffin-embedded liver tissues, we demonstrated first the correlation between the average TRF values evaluated by Southern blotting and the relative telomere intensities assessed by Q-FISH, and justified the application of Q-FISH. Small deviations in some cases can be attributed to the variability of telomere lengths among the various types of cells in the liver. Specifically, during chronic liver injury, hepatocytes proliferate in a process of regeneration and telomere regions are shortened progressively, while those of the infiltrating lymphocytes are shortened less because of their weak telomerase activity [9,10]. Sinusoidal cells are also reported to escape from progressive telomere shortening in the regenerating process [9,10]. Because Q-FISH enables us to measure accurately the telomere length of each cell, it is a particularly useful method to apply to diseased liver tissues, which consist of several types of cells with different telomere lengths.

Most human somatic cells can undergo only a limited number of divisions in vitro because the telomeres are shortened with each cell division, leading to cellular senescence. In cancer cells, the activation of telomerase results in the maintenance or elongation of telomeres and enables unlimited numbers of cell divisions [17]. However, little is known about the alteration of telomere length during tumor growth in vivo. Because tumor size is supposed to reflect the number of cancer cell divisions, we studied the relationship between telomere length and tumor size. Previously, only a few reports have mentioned the relationship between tumor size and telomere length, and most of them only compared telomere lengths in tumors and non-tumorous tissues [18–20]. In one paper, the authors reported that the telomeres of HCCs larger than 30 mm in size were significantly shorter than those of smaller tumors [21]. This can partly explain our data from group A tumors, whose telomere lengths correlated negatively with tumor size. But other authors have reported that there is no significant correlation between telomere length and tumor size [22]. We considered that, in the group A tumors, the effect of telomere maintenance and elongation was not as much as the shortening effect of cell

division and, therefore, they remain tumor size-dependent. This is also supported by our finding that the telomerase activity in group A tumors was significantly lower than that in group B tumors. To our knowledge, our paper is the first to categorize HCCs into two groups, based on whether or not the telomere length is dependent on tumor size.

The group A tumors, whose telomere lengths correlated negatively with tumor size, were of significantly less advanced stage and showed lower telomerase and proliferative activities than the group B tumors. This result indicates that the tumors are less aggressive while the telomere lengths remain dependent on tumor size but they gain more growth advantage to resist cellular senescence once the telomere lengths become size-independent. In previous reports, when HCCs grew larger than 3 cm in size, they frequently gained further malignant features [23]. This is in good agreement with our conclusion that all tumors of 5 cm in size or larger showed size-independent telomere lengths, accompanied by highly malignant clinicopathological features.

Telomere length has not been used widely as a biological marker for HCCs, probably because conventional Southern blot analysis requires more than 10^5 cells and the application is limited to surgically resected materials. Furthermore, prior to our report, there was no report on the association between telomere length and the clinicopathological features of HCCs. Because Q-FISH is generally applicable to biopsied materials, clarifying the telomere length of each cell, it is considered to be a potentially helpful method for evaluating the growth advantage of HCCs from the viewpoint of size-independence of telomere length.

References

[1] E.H. Blackburn, Structure and function of telomeres, Nature 350 (1991) 569–573.

[2] M.Z. Levy, R.C. Allsopp, A.B. Futcher, C.W. Greider, C.B. Harley, Telomere end-replication problem and cell aging, J. Mol. Biol. 225 (1992) 951–960.

[3] H. Aikata, H. Takaishi, Y. Kawakami, S. Takahashi, M. Kitamoto, T. Nakanishi, Y. Nakamura, F. Shimamoto, G. Kajiyama, T. Ide, Telomere reduction in human liver tissues with age and chronic inflammation, Exp. Cell Res. 256 (2000) 578–582.

[4] A. Nishimoto, N. Miura, I. Horikawa, H. Kugoh, Y. Murakami, S. Hirohashi, H. Kawasaki, A.F. Gazdar, J.W. Shay, J.C. Barrett, M. Oshimura, Functional evidence for a telomerase repressor gene on human chromosome 10p15.1, Oncogene 20 (2001) 828–835.

[5] A.K. Meeker, W.R. Gage, J.L. Hicks, I. Simon, J.R. Coffman, E.A. Platz, G.E. March, A.M. De Marzo, Telomere length assessment in human archival tissues: combined telomere fluorescence in situ hybridization and immunostaining, Am. J. Pathol. 160 (2002) 1259–1268.

[6] S. Ferlicot, N. Youssef, D. Feneux, F. Delhommeau, V. Paradis, P. Bedossa, Measurement of telomere length on tissue sections using quantitative fluorescence in situ hybridization (Q-FISH), J. Pathol. 200 (2003) 661–666.

[7] V. Kapoor, W.G. Telford, Telomere length measurement by fluorescence in situ hybridization and flow cytometry, Methods Mol. Biol. 263 (2004) 385–398.

[8] J.N. O'Sullivan, J.C. Finley, R.A. Risques, W.T. Shen, K.A. Gollahon, A.H. Moskovitz, S. Gryaznov, C.B. Harley, P.S. Rabinovitch, Telomere length assessment in tissue sections by quantitative FISH: image analysis algorithms, Cytometry 58A (2004) 120–131.

[9] V. Paradis, N. Youssef, D. Dargere, N. Ba, F. Bonvoust, J. Deschatrette, P. Bedossa, Replicative senescence in normal liver, chronic hepatitis C, and hepatocellular carcinomas, Hum. Pathol. 32 (2001) 327–332.

[10] S.U. Wiemann, A. Satyanarayana, M. Tsahuridu, H.L. Tillmann, L. Zender, J. Klempnauer, P. Flemming, S. Franco, M.A. Blasco, M.P. Manns, K.L. Rudolph, Hepatocyte telomere shortening and senescence are general markers of human liver cirrhosis, FASEB J. 16 (2002) 935–942.

[11] N.W. Kim, F. Wu, Advances in quantification and characterization of telomerase activity by the telomeric repeat amplification protocol (TRAP), Nucleic Acids Res. 25 (1997) 2595–2597.

[12] G.M. Church, W. Gilbert, Genomic sequencing, Proc. Natl. Acad. Sci. USA 81 (1984) 1991–1995.

[13] Liver Cancer Study Group of Japan. Classification of primary liver cancer, Tokyo: Kanehara&Co., Ltd, 1997.

[14] N.T. van Heek, A.K. Meeker, S.E. Kern, C.J. Yeo, K.D. Lillemoe, J.L. Cameron, G.J. Offerhaus, J.L. Hicks, R.E. Wilentz, M.G. Goggins, A.M. De Marzo, R.H. Hruban, A. Maitra, Telomere shortening is nearly universal in pancreatic intraepithelial neoplasia, Am. J. Pathol. 161 (2002) 1541–1547.

[15] A.K. Meeker, J.L. Hicks, E. Gabrielson, W.M. Strauss, A.M. De Marzo, P. Argani, Telomere shortening occurs in subsets of normal breast epithelium as well as in situ and invasive carcinoma, Am. J. Pathol. 164 (2004) 925–935.

[16] E. Montgomery, P. Argani, J.L. Hicks, A.M. DeMarzo, A.K. Meeker, Telomere lengths of translocation-associated and non-translocation-associated sarcomas differ dramatically, Am. J. Pathol. 164 (2004) 1523–1529.

[17] N. Miura, I. Horikawa, A. Nishimoto, H. Ohmura, H. Ito, S. Hirohashi, J.W. Shay, M. Oshimura, Progressive telomere shortening and telomerase reactivation during hepatocellular carcinogenesis, Cancer Genet. Cytogenet. 93 (1997) 56–62.

[18] K. Ohashi, M. Tsutsumi, Y. Nakajima, K. Kobitsu, H. Nakano, Y. Konishi, Telomere changes in human hepatocellular carcinomas and hepatitis virus infected noncancerous livers, Cancer 77 (1996) 1747–1751.

[19] Y. Urabe, K. Nouso, T. Higashi, H. Nakatsukasa, N. Hino, K. Ashida, N. Kinugasa, K. Yoshida, S. Uematsu, T. Tsuji, Telomere length in human liver diseases, Liver 16 (1996) 293–297.

[20] H. Kojima, O. Yokosuka, F. Imazeki, H. Saisho, M. Omata, Telomerase activity and telomere length in hepatocellular carcinoma and chronic liver disease, Gastroenterology 112 (1997) 493–500.

[21] K. Ohashi, M. Tsutsumi, K. Kobitsu, T. Fukuda, T. Tsujiuchi, E. Okajima, S. Ko, Y. Nakajima, H. Nakano, Y. Konishi, Shortened telomere length in hepatocellular carcinomas and corresponding background liver tissues of patients infected with hepatitis virus, Jpn. J. Cancer Res. 87 (1996) 419–422.

[22] G.T. Huang, H.S. Lee, C.H. Chen, L.L. Chiou, Y.W. Lin, C.Z. Lee, D.S. Chen, J.C. Sheu, Telomerase activity and telomere length in human hepatocellular carcinoma, Eur. J. Cancer 34 (1998) 1946–1949.

[23] M. Ebara, M. Ohto, T. Shinagawa, N. Sugiura, K. Kimura, S. Matsutani, M. Morita, H. Saisho, Y. Tsuchiya, K. Okuda, Natural history of minute hepatocellular carcinoma smaller than three centimeters complicating cirrhosis. A study in 22 patients, Gastroenterology 90 (1986) 289–298.